5-17-2023

Structural Relationships Across the Sevier Gravity Slide of Southwest Utah and Implications for Catastrophic Translation and Emplacement Processes of Long Runout Landslides

Michael J. Braunagel

William Ashley Griffith

Robert F. Biek

David B. Hacker

Peter D. Rowley

See next page for additional authors

Recommended Citation

R. F., Hacker, D. B., Rowley, P. D., Malone, D. H., et al. (2023). Structural relationships across the Sevier gravity slide of southwest Utah and implications for catastrophic translation and emplacement processes of long runout landslides. Geochemistry, Geophysics, Geosystems, 24, e2022GC010783. https://doi.org/10.1029/2022GC010783.

Geochemistry, Geophysics, Geosystems®

AGU ADVANCING EARTH AND SPACE SCIENCE

RESEARCH ARTICLE
10.1029/2022GC010783

Key Points:

- Field observations at the long-runout Sevier gravity slide indicate high-velocity emplacement aided by suprahydrostatic fluid pressures
- Slip localization and low-permeability volcanic rocks promote effective dynamic weakening mechanisms early in translation history
- Increasing damage, permeability, and slip delocalization result in deceleration and cessation of the Sevier gravity slide

Correspondence to:
M. J. Braunagel,
braunagel.2@osu.edu

Citation:
Braunagel, M. J., Griffith, W. A., Biek, R. F., Hacker, D. B., Rowley, P. D., Malone, D. H., et al. (2023). Structural relationships across the Sevier gravity slide of southwest Utah and implications for catastrophic translation and emplacement processes of long runout landslides. *Geochemistry, Geophysics, Geosystems*, *24*, e2022GC010783. https://doi.org/10.1029/2022GC010783

Received 10 NOV 2022
Accepted 8 MAR 2023

Structural Relationships Across the Sevier Gravity Slide of Southwest Utah and Implications for Catastrophic Translation and Emplacement Processes of Long Runout Landslides

Michael J. Braunagel[1], W. Ashley Griffith[1], Robert F. Biek[7], David B. Hacker[2], Peter D. Rowley[3], David H. Malone[4], Danika Mayback[1], Tiffany A. Rivera[5], Zachary Loffer[2], and Zachary D. Smith[1,6]

[1]School of Earth Sciences, The Ohio State University, Columbus, OH, USA, [2]Department of Earth Sciences, Kent State University, Kent, OH, USA, [3]Geologic Mapping Inc., New Harmony, UT, USA, [4]Department of Geology-Geography, Illinois State University, Normal, IL, USA, [5]Department of Geology, Westminster College, Salt Lake City, UT, USA, [6]Earth and Planetary Science, University of California at Berkeley, Berkeley, CA, USA, [7]Retired, Utah Geological Survey, Salt Lake City, UT, USA

Abstract The physical processes that facilitate long-distance translation of large-volume gravity slides remain poorly understood. To better understand these processes and the controls on runout distance, we conducted an outcrop and microstructural characterization of the Sevier gravity slide across the former land surface and summarize findings of four key sites. The Sevier gravity slide is the oldest of three mega-scale (>1,000 km^2) collapse events of the Marysvale volcanic field (Utah, USA). Field observations of intense deformation, clastic dikes, pseudotachylyte, and consistency of kinematic indicators support the interpretation of rapid emplacement during a single event. Furthermore, clastic dikes and characteristics of the slip zone suggest emplacement involved mobilization and pressurized injection of basal material. Across the runout distance, we observe evidence for progressive slip delocalization along the slide base. This manifests as centimeter- to decimeter-thick cataclastic basal zones and abundant clastic dikes in the north and tens of meters thick basal zones characterized by widespread deformation of both slide blocks and underlying rock near the southern distal end of the gravity slide. Superimposed on this transition are variations in basal zone characteristics and slide geometry arising from interactions between slide blocks during dynamic wear and deposition processes and pre-existing topography of the former land surface. These observations are synthesized into a conceptual model in which the presence of highly pressurized fluids reduced the frictional resistance to sliding during the emplacement of the Sevier gravity slide, and basal zone evolution controlled the effectiveness of dynamic weakening mechanisms across the former land surface.

Plain Language Summary Large-volume volcanic landslides pose a low-frequency but high-impact natural hazard due to both their massive size and long-runout distances that exceed predictions grounded in simple sliding models. Studying the deposits of past long-runout landslides provides insight into the physical processes that reduce friction and aid movement of slide material for long distances over the land surface. We describe the deformation styles observed in the basal zone of the gigantic Sevier gravity slide of southwestern Utah to build a conceptual model for the physical processes associated with the slide's emplacement. Field observations indicate high fluid pressures beneath the slide promoted high-velocity sliding. During slip, mechanical breakdown of rocks exposed at the slide plane and deposition of wear products allowed pressurized fluids to escape the basal zone and resulted in deceleration of the slide.

1. Introduction

The Marysvale gravity slide complex (MGSC) of southwestern Utah consists of three mega-scale collapse events (Figure 1) that record gravitational failure and sector collapse of the southern flank of the Marysvale volcanic field (MVF) (Biek et al., 2015, 2019; Hacker et al., 2014). Collectively, the MGSC structures cover approximately 8,000 km^2, ranking each individually among Earth's largest terrestrial landslides. The continuity and consistency of kinematic indicators, the presence of deformation features including pseudotachylyte, clastic dikes, and localized hydrothermal alteration within the basal deformation zone, all indicate that each collapse structure represents a single high-velocity emplacement event (Biek et al., 2015, 2019; Hacker et al., 2014). The MGSC structures are of similar volume and runout distance to the Heart Mountain slide of Wyoming (Craddock et al., 2009; Malone et al., 2014, 2017), the only other known mega-scale terrestrial gravity slide.

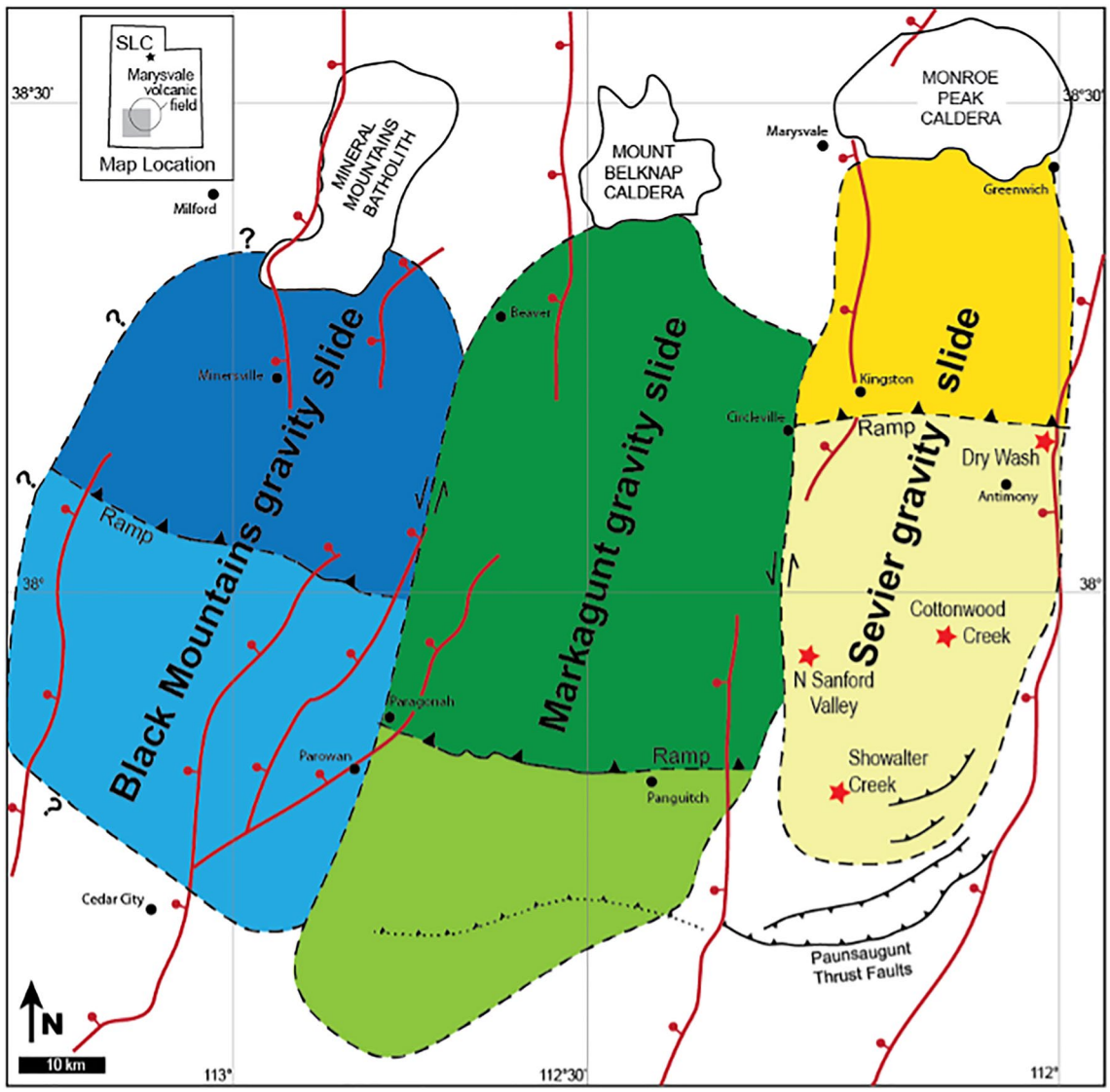

Figure 1. Generalized map of the Marysvale gravity slide complex showing the estimated spatial extent of each slide structure based on current mapping. The breakaway (dark) and runout (light) segments of each slide are separated by a ramp where the basal slip surface cut upwards from the subsurface detachment plane to the former land surface. The four sites described in this study of the former land surface segment of the Sevier gravity slide are shown as stars. Red lines show major Basin and Range normal faults. The breakaway area of each slide is overprinted by three of the largest volcanic features in the MVF, namely the Monroe Peak and Mount Belknap calderas, and the Mineral Mountains batholith. Inset shows the location of map (gray box) and approximate extent of Marysvale volcanic field rocks.

Of the three MGSC structures, we focus on the eastern Sevier gravity slide (SGS) due to the near continuous exposure of the basal zone created by subsequent Basin and Range normal faults striking parallel to the slide transport direction (Figure 1). Current mapping indicates that the SGS reaches as far northward as the Monroe Peak caldera (Figure 1), and the most distal deposits are observed ~80 km to the south at Flake Mountain (Biek et al., 2019). In total, the SGS experienced at least 35 km of translation over the former land surface south of the ramp (Figure 1) (Biek et al., 2019).

Landslides exhibit an inverse relationship between slide volume and the effective coefficient of friction, expressed as the ratio of runout distance to initial vertical fall height (Collins & Melosh, 2003; Johnson et al., 2016; Legros, 2002) (Figure 2). For long-runout landslides with volumes exceeding ~1 km^3, the effective coefficient of friction implied by this relationship is lower than typical values for rocks (Byerlee, 1978). The MGSC structures follow this trend (Figure 2) with an effective friction coefficient <<0.1. Based on field observations, laboratory testing, and numerical modeling, numerous mechanisms have been proposed to reduce

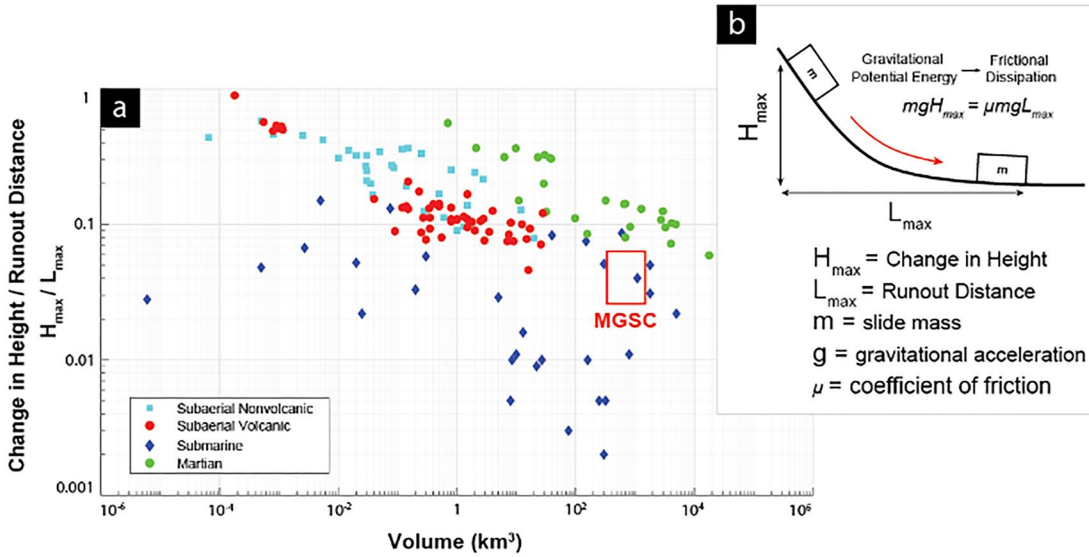

Figure 2. (a) Inverse relationship between effective coefficient of friction calculated from the energy balance of a sliding rigid block illustrated in (b) and landslide volume (data from Legros, 2002). The three MGSC structures individually fall within the red box based on mapping constraints provided by Biek et al. (2015, 2019).

sliding friction of long-runout landslides below typical values for rocks and explain long runout (e.g., Shaller & Smith-Shaller, 1996). These include bulk fluidization mechanisms based in the physics of granular flow, such as acoustic fluidization (Johnson et al., 2016; Melosh, 1979) and fragmentation and spreading (Davies & McSaveney, 2009), gas fluidization of basal gravels in the presence of carbon dioxide (Aharonov & Anders, 2006; Anders et al., 2010), and mechanisms that lubricate the slip surface to reduce the frictional resistance to sliding. At high slip velocities, a number of physiochemical processes documented by Di Toro et al. (2011) were observed to result in dramatic reductions in friction during rotary shear experiments of various lithologies. In long-runout landslides, mechanisms including air lubrication (Shreve, 1968), carbonate decomposition and pressurization of carbon dioxide (Goren et al., 2010; Mitchell et al., 2015), and thermal pressurization of pore water (Goren & Aharonov, 2007) have been proposed as mechanisms for reducing frictional contact between a slide mass and the underlying substrate during emplacement. Air lubrication has been since demonstrated to be unable to support the load of a landslide due to rapid escape through the slide mass, but water is a more efficient medium due to its higher density, viscosity, and incompressibility (Legros, 2002). While other mechanisms are physically viable, thermal pressurization of water in the basal zone of long runout landslides is a highly likely process for reducing the frictional resistance to sliding as it can occur in any lithology so long as the pore space is saturated and the rocks have generally low permeability (e.g., Goren & Aharonov, 2009; Viesca & Garagash, 2015).

The SGS is an exceptional field laboratory to study the mechanics of landslide initiation, translation, and cessation due to the near continuous exposure of the basal zone and abundance of geologic mapping completed in the region (e.g., Biek et al., 2019; Rowley et al., 2002). Moreover, the general north to south transport direction of the SGS lies parallel to the strike of older thrust faults and folds produced by the west to east shortening of the Sevier orogeny, resulting in slide-related transport that is generally orthogonal to that of the pre-existing fold and thrust belt. By identifying systematic trends in the basal structure of the SGS, deformation styles can be tied to slide mechanics to build a conceptual model that describes the mechanisms that control both high-velocity transport and ultimate cessation of the SGS. Furthermore, field observations highlight the complexity that arises from translation across the former land surface, in contrast to block models often used to simulate landslide emplacement.

2. Geologic Setting

Igneous activity in the MVF during the Oligocene to early Miocene consisted primarily of subduction-derived andesitic magmatism. Most volcanic products are assigned to the Mount Dutton Formation in the southern portion of the volcanic field and Bullion Canyon Volcanics in the north. Collectively, these formations are a >2 km

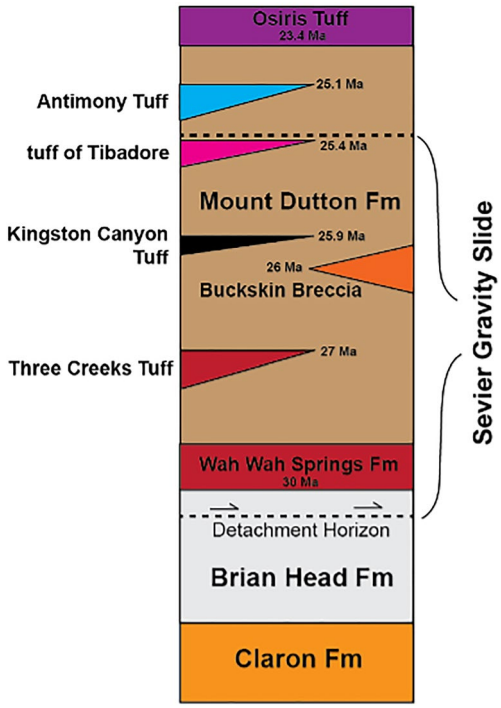

Figure 3. Simplified stratigraphic section of the Sevier Plateau showing main units involved in the Sevier gravity slide. Ages of volcanic units from Biek et al. (2019) and references therein. Not to scale.

thick intertonguing and cross cutting mix of lahars, lava flows, welded tuffs, and shallow magmatic intrusions derived from clustered stratovolcanoes that were active between 30 and 22 Ma (Anderson & Rowley, 1975; Palmer & Walton, 1990; Rowley et al., 1998, 2002). Distinctive interbedded ash flow tuffs are present throughout the volcanic succession (Figure 3) and include the Wah Wah Springs, Three Creeks Tuff, Buckskin Breccia, and Kingston Canyon Tuff (Rowley et al., 1998, 2002).

The Wah Wah Springs Formation is a crystal-rich dacite tuff that erupted ~30 Ma from the Indian Peak Caldera along the present-day Utah-Nevada border (Best et al., 2013; Biek et al., 2015; Rowley et al., 1994). The ~27 Ma Three Creeks Tuff Member of the Bullion Canyon Volcanics was produced locally by the eruption of the Three Creeks caldera located in the northern MVF (Steven et al., 1984). The Three Creeks Tuff is texturally and compositionally similar to the Wah Wah Springs Formation, making the two difficult to distinguish in structurally complicated areas. The Buckskin Breccia is a 26 Ma lithic tuff originating from an eruptive episode of the nearby Spry Intrusion (Rowley et al., 1994), and the Kingston Canyon Tuff Member of the Mount Dutton Formation is a densely welded, crystal poor trachytic tuff with a basal vitrophyre sourced from the northern MVF (Fleck et al., 1975). Minor volcanic tuffs including the tuff of Tibadore deformed within the SGS and the undeformed 25 Ma Antimony Tuff Member of the Mount Dutton Formation overlying the SGS (Figure 3) constrain the age of emplacement to ~25 Ma (Biek et al., 2019).

Volcanic units overlie the late Eocene-Oligocene Brian Head Formation (Figure 3), a white to gray mudstone, sandstone, and conglomerate (Anderson & Rowley, 1975; Sable & Maldonado, 1997). This unit records the onset of volcanism in the region and contains abundant volcanic ash weathered to smectite, a swelling clay with high susceptibility to failure (Biek et al., 2015; Ferri et al., 2011). Brian Head strata conformably overlie Paleocene(?) to middle Eocene limestone, mudstone, sandstone, and conglomerate of the Claron Formation (Anderson & Rowley, 1975; Sable & Maldonado, 1997).

3. Methods

We document structural relationships across the SGS at four sites on the former land surface segment, including (from north to south) Dry Wash, Cottonwood Creek, North Sanford Valley, and Showalter Creek (Figure 1). At each site, we identified the location of the basal slide plane and measured the orientation of structural elements including bedding, the basal slip surface, and secondary slip surfaces. Where possible, we also identified the slip direction and sense of slip indicated by slickensided surfaces and sense-of-shear indicators. All structural data are plotted using Stereonet 11 (Cardozo & Allmendinger, 2013) and kinematic inversions of SGS-related faulting are calculated using FaultKin 8 (Marrett & Allmendinger, 1990).

At each of the four sites, 3D outcrop-scale models were generated using structure-from-motion photogrammetry. This technique identifies the three-dimensional location of a set of given points shared in overlapping photos relative to the camera position, allowing images to be stitched together in 3D space (Bemis et al., 2014; Pringle et al., 2006; Smith & Maxwell, 2021). In this study, photographs were obtained using a DJI Mavic 2 uncrewed aerial vehicle (UAV) with a Hasselblad camera system. Survey design of each exposure included a minimum of three flight lines, each with different altitudes, to capture photos at various camera angles with at least 70% overlap between adjacent photos. During each flight line, the internal GPS in the UAV records position and orientation data of each photo captured, with a positional error generally <5 m. Virtual 3D outcrop models are generated from the UAV photos using AgiSoft Metashape. This software uses the UAV position data for each photo to estimate the position of the camera during processing and tie points between overlapping photos to estimate distance and generate a dense point cloud and texture. Models generated using the position data generally have a high degree of precision, allowing for reliable structural measurements, and relevant data are extracted from the outcrop models using Cloud Compare (Thiele et al., 2017).

Oriented samples of basal material and overlying upper plate rock were set in blue epoxy, thin sectioned, and analyzed using a Leica DFC290 camera mounted to a Leitz transmitted light microscope. From thin sections, we calculate the grain size distribution following Frost et al. (2009) to estimate the degree of comminution the material experienced during emplacement of the SGS and overall maturity of the shear zone (Blenkinsop, 1991; Sammis & King, 2007). Boundaries of quartz and feldspar grains in the basal layer were delineated from black and white thin section photos using the adaptive threshold method of Otsu (1979) in Matlab. These specific grains were selected for analysis due to the high contrast between the optically bright grains and the darker-colored matrix in photos captured with the Leica DFC290 camera. Identified grains were sorted into groups defined by average diameter ranging between 5 μm and 4 mm, with each bin differing from the previous by a factor of two. The power law line of best fit to these data plotted on log-log plots of grain size versus grain density yields the two-dimensional grain size distribution or fractal dimension (D_2) of the material (Frost et al., 2009; Sammis & King, 2007).

4. Observations

4.1. Dry Wash

Dry Wash (38.159°, −111.933°) is the northernmost site of this study and closest to the inferred location of the ramp to the north (Figure 1); however, the basal slide plane is not well exposed north of this site. This site exposes ∼50 m of allochthonous volcanic mudflow breccia of the Mount Dutton Formation and Three Creeks Tuff above in-place Buckskin Breccia and unnamed flat-lying yellow, Eocene-aged fluvial strata (Figure 4a) (Biek et al., 2019). The Three Creeks Tuff above the Buckskin Breccia at this site provides an older-on-younger stratigraphic relationship characteristic of the former land surface segments of the adjacent Markagunt gravity slide (e.g., Hacker et al., 2014) and smaller-scale collapse structures in the nearby Iron Axis region of Utah (e.g., Hacker et al., 2002). The resistant upper surface of the Buckskin Breccia forms a ledge that marks the location of the basal slide plane throughout the wash, while the damaged lowermost portion of the slide block at Dry Wash is easily weathered and poorly exposed.

The basal surface at Dry Wash is subhorizontal (153°/04° W; Figure 4b), and polished with well-developed striations (Figure 4c) that indicate transport directions of the SGS spanning 168° to 180° (Figure 4b). Above the slide plane, an approximately 2 cm to 0.5 m thick layer of deposited wear products (basal layer, as described by Malone et al., 2014; Mayback et al., 2022) is present (Figure 4a). Allochthonous units are shattered and sheared, and stratigraphic layering in the mudflows is contorted and difficult to discern with confidence, with lithologic boundaries that display pinch and swell-like geometries (Figure 4d). We assign the SGS upper plate at Dry Wash to the mixed facies (Komorowski et al., 1991; Siebert, 2002). The upper plate contains numerous red to gray, well indurated, subvertical clastic dikes (Figure 4e) up to 0.3 m in width and in some cases exceeding tens of meters in length. The injected material is matrix-supported and contains clasts up to a few centimeters in diameter. Flow indicators, branching patterns, and opening distributions that thin upwards indicate dominant upward propagation of dikes from the basal surface. However, while the contact between clastic dikes and the basal layer is not exposed, textural and compositional differences between the clastic dike material and the basal wear layer exposed elsewhere along the basal zone suggest that the dikes were formed earlier during emplacement and were then transported to this location, similar to observations of clastic dikes at the base of the adjacent Markagunt gravity slide (Mayback et al., 2022).

4.2. Cottonwood Creek

The ∼75 m thick allochthonous succession at Cottonwood Creek (37.960°, −112.071°) contains the most complete volcanic section observed in the SGS, including Wah Wah Springs Formation, Three Creeks Tuff, Kingston Canyon Tuff, and Mount Dutton alluvial facies mudflows in a normal stratigraphic sequence (Figure 5a). The basal zone at Cottonwood Creek is largely covered by colluvium and poorly exposed, but where present, an ∼0.5–1 m thick drab green to brown basal layer overlies the conglomerate of the upper Brian Head Formation (Figures 5a and 5c). The basal layer contains sub-to well-rounded igneous and quartzite clasts and abundant biotite. Lower plate Brian Head Formation is generally undisturbed, except for local jigsaw-style fractured clasts immediately beneath the contact and sheared clasts at the slide surface (Figure 5d). Jigsaw fractures, characterized by intense fracturing with minimal rotation and disarticulation of fragments leaving a fitted fabric to

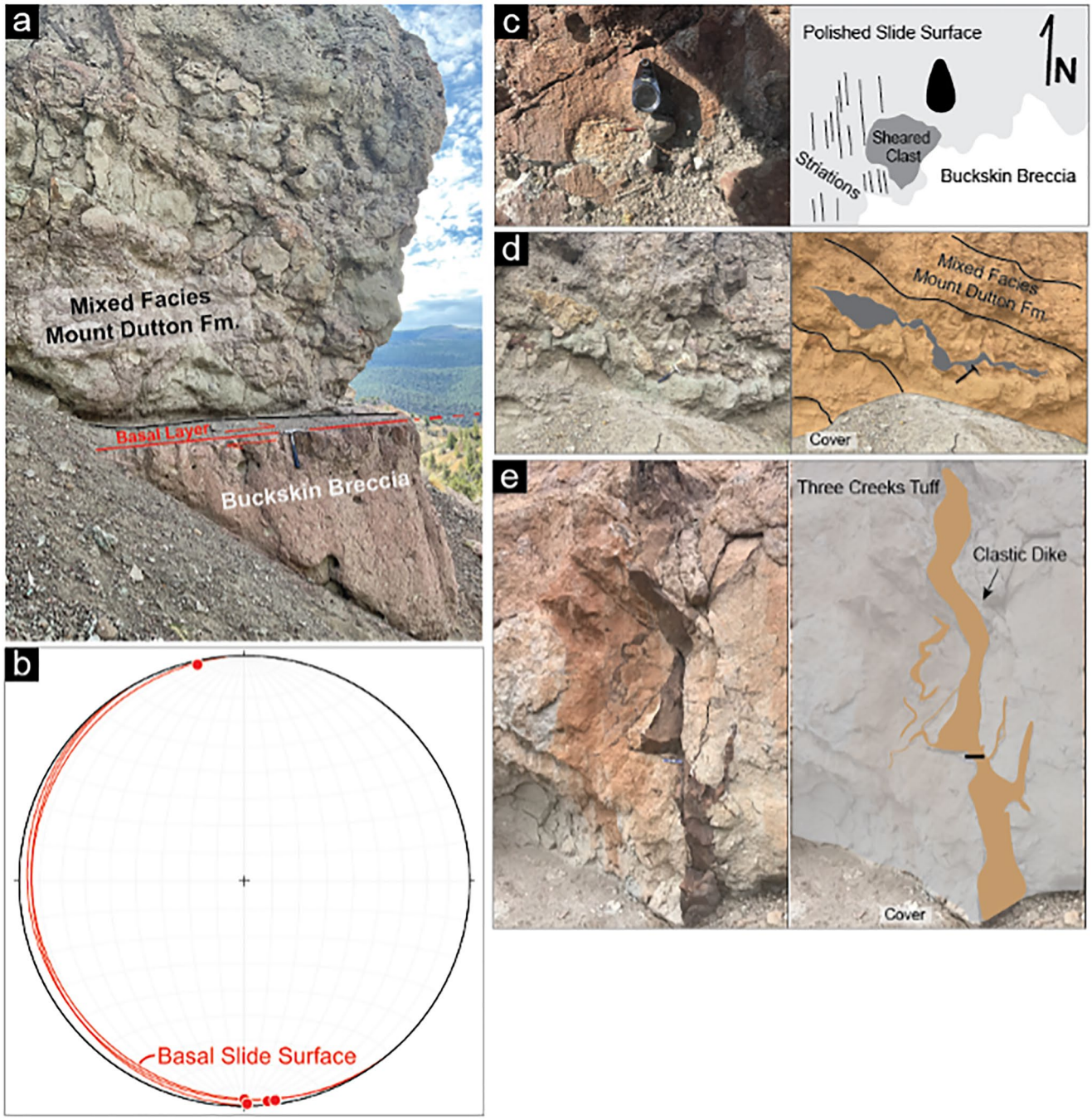

Figure 4. Sevier gravity slide deformation at Dry Wash. (a) Exposure of the basal zone showing the location of the basal slip surface and adjacent lithologies. (b) Equal area stereographic projection showing attitudes of the subhorizontal basal slip surface and southward directed striations observed at Dry Wash. (c) Polished upper surface of the Buckskin Breccia and striations record southward transport. (d) Stretched and contorted layering in the upper plate. (e) Clastic dikes propagate upwards into allochthonous Three Creeks Tuff. The contact of dikes with basal layer is not observed, but textural and compositional differences suggest the dikes did not form from the local basal material.

damaged clasts, are commonly observed in volcanic debris-avalanche deposits (Shaller et al., 2020; Shreve, 1968; Malone, 1995). Bedding in the underlying Brian Head Formation remains subhorizontal. The basal surface dips gently toward the east (013°/05°E) with striations indicating transport toward 162° to 185° (Figure 5b).

Allochthonous material overlying the slide plane contains damaged Wah Wah Springs and Mount Dutton Formations. Boundaries between the rock units are difficult to discern, suggesting significant mixing of the materials

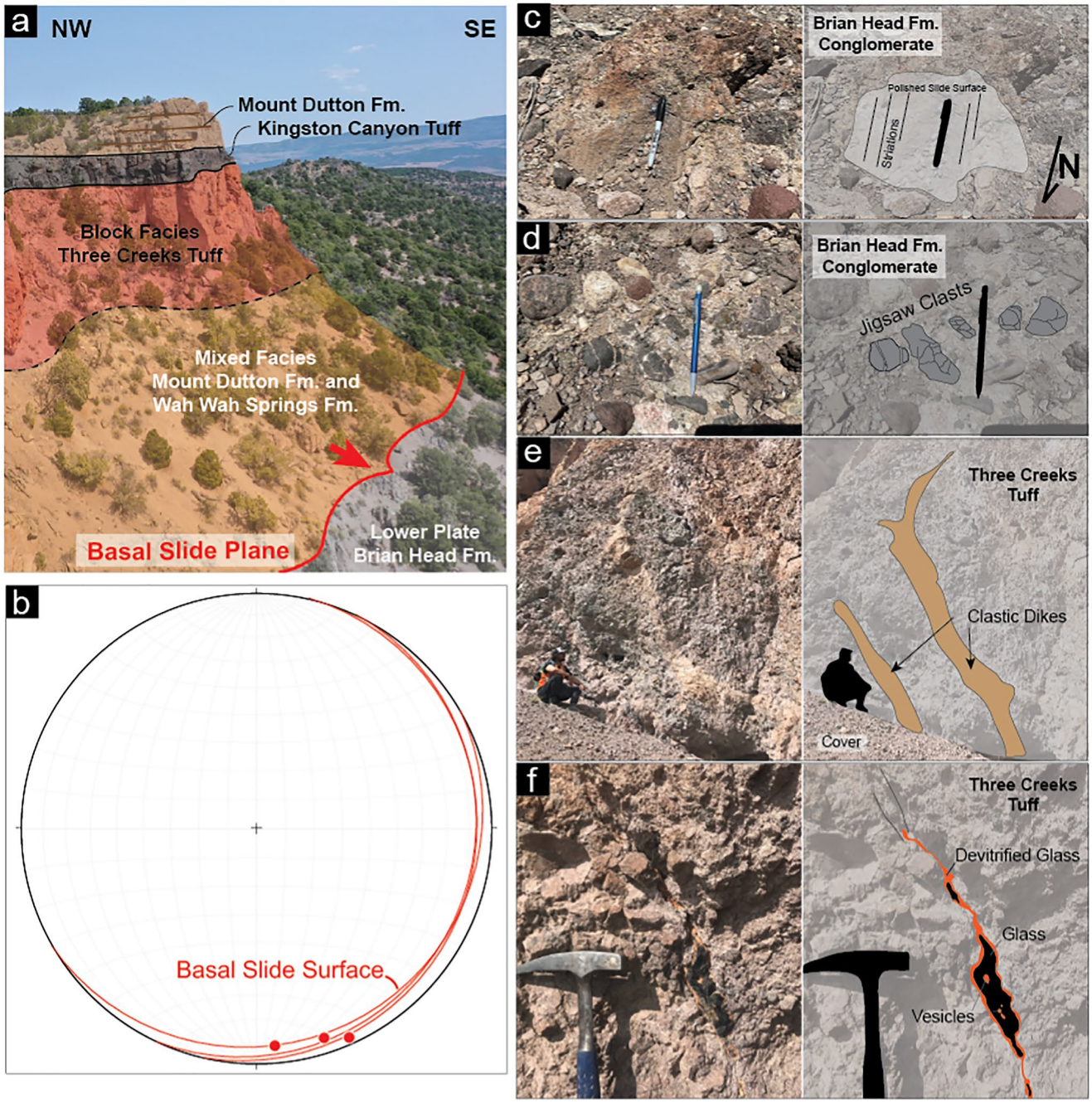

Figure 5. Sevier gravity slide deformation at Cottonwood Creek. (a) Stratigraphy of involved rocks. A complete stratigraphic section from the Wah Wah Springs Formation into the Mount Dutton Formation is preserved in the upper plate. The intensely deformed mixed facies immediately overlying the basal slide surface grades upwards into more intact block facies near the upper portions of the exposure. (b) Equal area stereographic projection of the subhorizontal basal slip surface and southward trending striations observed at Dry Wash. (c) Subtle striations and sheared clasts in the Brian head Formation mark the basal slide plane. (d) Jigsaw fractured clasts contained within the Brian Head Formation immediately below the basal slip surface. (e) Clastic dikes propagate upwards into the cataclastically deformed Three Creeks Tuff. (f) Dark glassy vein in the Three Creeks Tuff interpreted as pseudotachylyte.

(Komorowski et al., 1991; Siebert, 2002). With increasing distance above the slide plane, upper plate units appear more intact, grading into the block facies (Siebert, 2002) from the more disrupted texture of the mixed facies. The Three Creeks Tuff is cataclastically deformed, but the upper contact with the Kingston Canyon Tuff basal vitrophyre is well-defined (Figure 5a) and the overlying Kingston Canyon Tuff and Mount Dutton Formation remain macroscopically intact (Figure 5a). There is no evidence of significant slide-related damage in these units

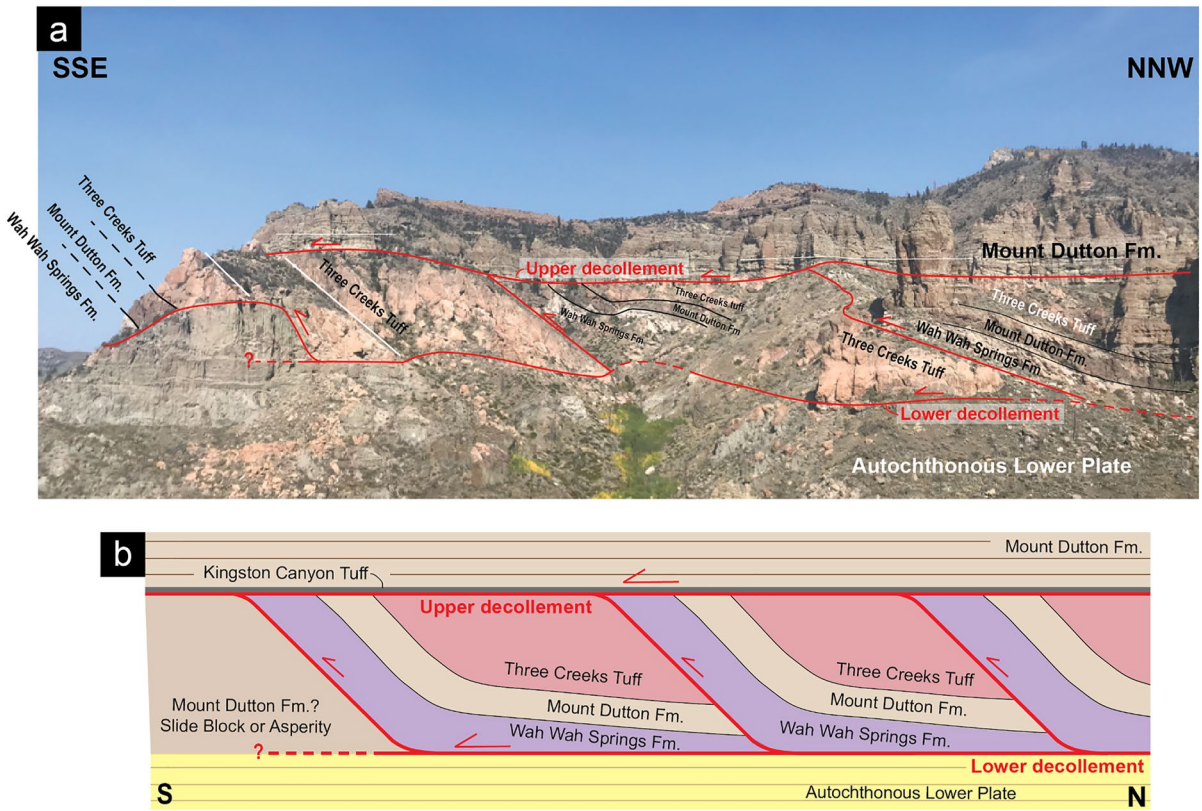

Figure 6. Outcrop scale map of deformation at North Sanford Valley annotated on field photo (a) and illustrated (b). Two subhorizontal decollements separate an imbricate thrust system containing a repeated sequence of Wah Wah Springs Formation, Three Creeks Tuff, and Mount Dutton Formation.

and the original stratigraphic layering in the mudflows is preserved. Bedding in the Mount Dutton Formation dips gently toward the northwest.

Some fractures in the well-exposed Three Creeks Tuff are filled with granular material similar in composition to the mixed facies zone and there are numerous clastic dikes that originate in the basal layer and intrude upper plate rocks (Figure 5e). These clastic dikes are generally thinner and less resistant to erosion than those observed at Dry Wash, suggesting differences in source material. Within the Three Creeks Tuff, we also observe a ∼2 cm thick, ∼1 m long, subvertical black glassy vein with outer contacts colored orange-red (Figure 5f). Similar glass-lined planes are observed in other exposures within the SGS, typically on surfaces within the Mount Dutton Formation.

4.3. North Sanford Valley

Exposures at the North Sanford Valley site (37.944°, −112.239°) are structurally complex, with a geometry resembling an imbricate floor-roof thrust system (Figure 6). In deeper areas of the valley, exposures of subhorizontal Brian Head Formation are overlain by a well-developed basal layer, marking the location of the lower decollement or floor of the thrust system that separates allochthonous rocks from lower plate Brian Head Formation. This decollement displays relief with amplitudes up to 10 m (Figure 6a), but generally is shallowly dipping toward the south (097°/12° S) with striations indicating transport toward 188° to 200° (Figure 7). We interpret this surface to be the lower contact of the SGS. In sharp contact with the basal layer, Wah Wah Springs Formation, Mount Dutton Formation, and Three Creeks Tuff dip toward the north at ∼40°. This panel repeats to the north along south-vergent imbricate thrust faults that splay upwards from the lower slide surface and ends to the south near the mouth of the valley. The imbricate thrust sequence ends here at a contact with a sheared and brecciated mass of gray to green, matrix-supported material containing large clasts of volcanic rock and rough subhorizontal fabric (Figure 6a). Overlying the repeating sequence of north dipping Wah Wah Springs Formation, Mount Dutton mudflows, and Three Creeks Tuff are subhorizontal Kingston Canyon Tuff and Mount Dutton Formation (Figure 6). This contact is marked by an abrupt change in attitude where north dipping units are

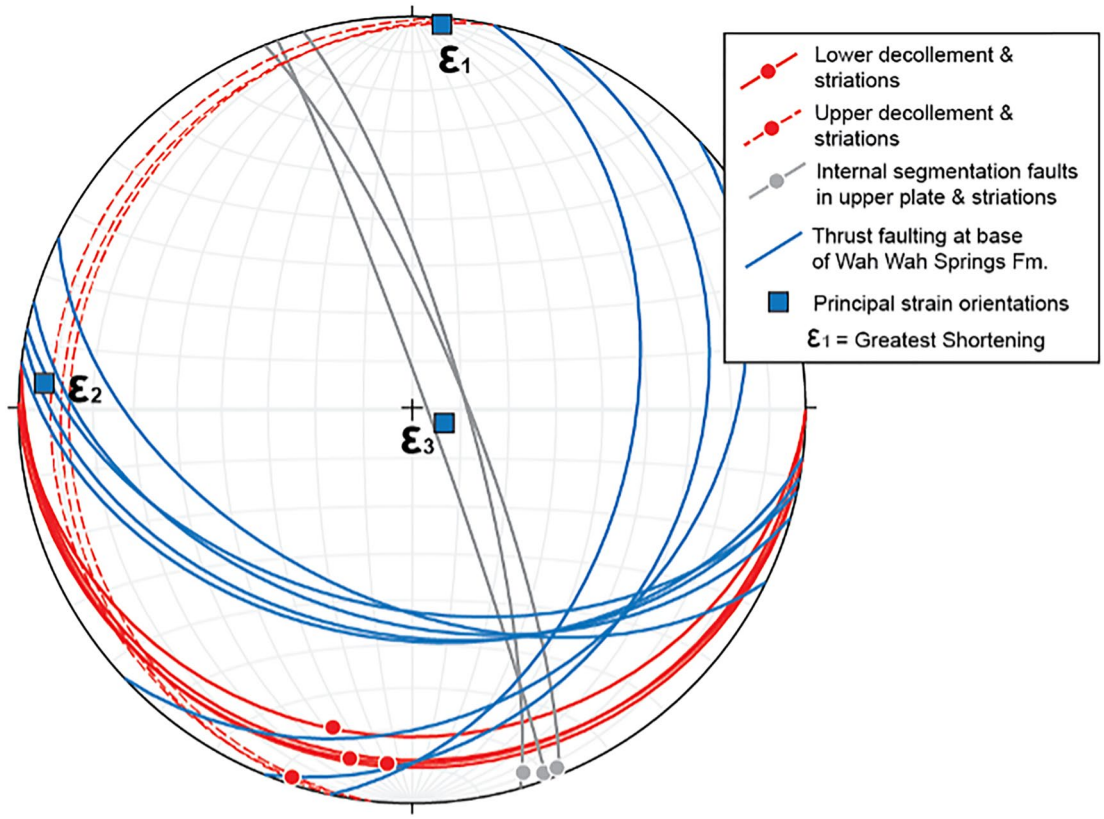

Figure 7. Equal area stereographic projection of the slip surfaces and internal deformation observed at the North Sanford Valley site. The lower decollement (solid red) is shallowly dipping toward the south with striations indicating generally southward transport of the slide block. The upper decollement (dashed red) is shallowly west dipping with striations toward ~200°. Kinematic inversions of steeply dipping internal slip surfaces (blue) are calculated assuming pure dip slip.

truncated at an upper decollement against the overlying subhorizontal surface (Figure 6). This surface is gently west dipping (186°/10° W) with striations indicating transport toward 198° (Figure 7). We interpret this contact as a second, stratigraphically higher slide surface that formed during the emplacement of the SGS.

The tan basal layer at the lower decollement is matrix supported and is between 0.5 and 2 m in thickness. It contains subangular to rounded volcanic clasts, some of which are pervasively fractured at the outer edges (Figure 8a), suggesting dilation and inflation (Schneider & Fisher, 1998). The basal layer has no particularly recognizable fabric at the outcrop scale, though contorted color banding is sub-parallel to the basal layer contacts (Figure 8b) consistent with layer parallel shear. Cobbles exposed at the slide surface are sheared and striated (Figure 8c), and the Wah Wah Springs Formation is cut by tan to green clastic dikes that intrude upwards from the basal surface (Figure 8d). Texture and composition similarities with the basal layer, continuity between dike and basal layer materials, and preserved flow structures within the dikes indicate clastic dikes formed locally. In thin section, the basal layer is poorly sorted, with 2–5 mm diameter igneous clasts and 0.5–1 mm grains of individual plagioclase, quartz, biotite, and opaques in a fine-grained matrix (Figure 9). The larger clasts and quartz grains are generally subrounded to subangular and quartz grains are optically uniform with no subgrain boundaries, deformation lamellae, or evidence of undulose extinction (Figures 9a–9g). Biotite and plagioclase crystals retain rectangular crystal habit and plagioclase grains display deformation twinning textures in cross-polarized light (Figures 9a, 9c and 9d). Grains do not display a clear preferred orientation.

The central area of the North Sanford Valley site containing north dipping, repeating sections of the Wah Wah Springs Formation, Mount Dutton Formation, and Three Creeks Tuff is pervasively fractured and sheared with macroscopic sense of shear indicators that are consistent with top toward the south deformation (Figure 8e). This suggests that, locally, top-to-the-south shear strain was distributed beyond the localized basal layer, and up into the upper plate rocks. Additionally, sub-vertical slip surfaces oriented at acute angles to the transport direction (164°/86° E) displaying horizontal striations toward 175° (Figure 7) are common throughout this section

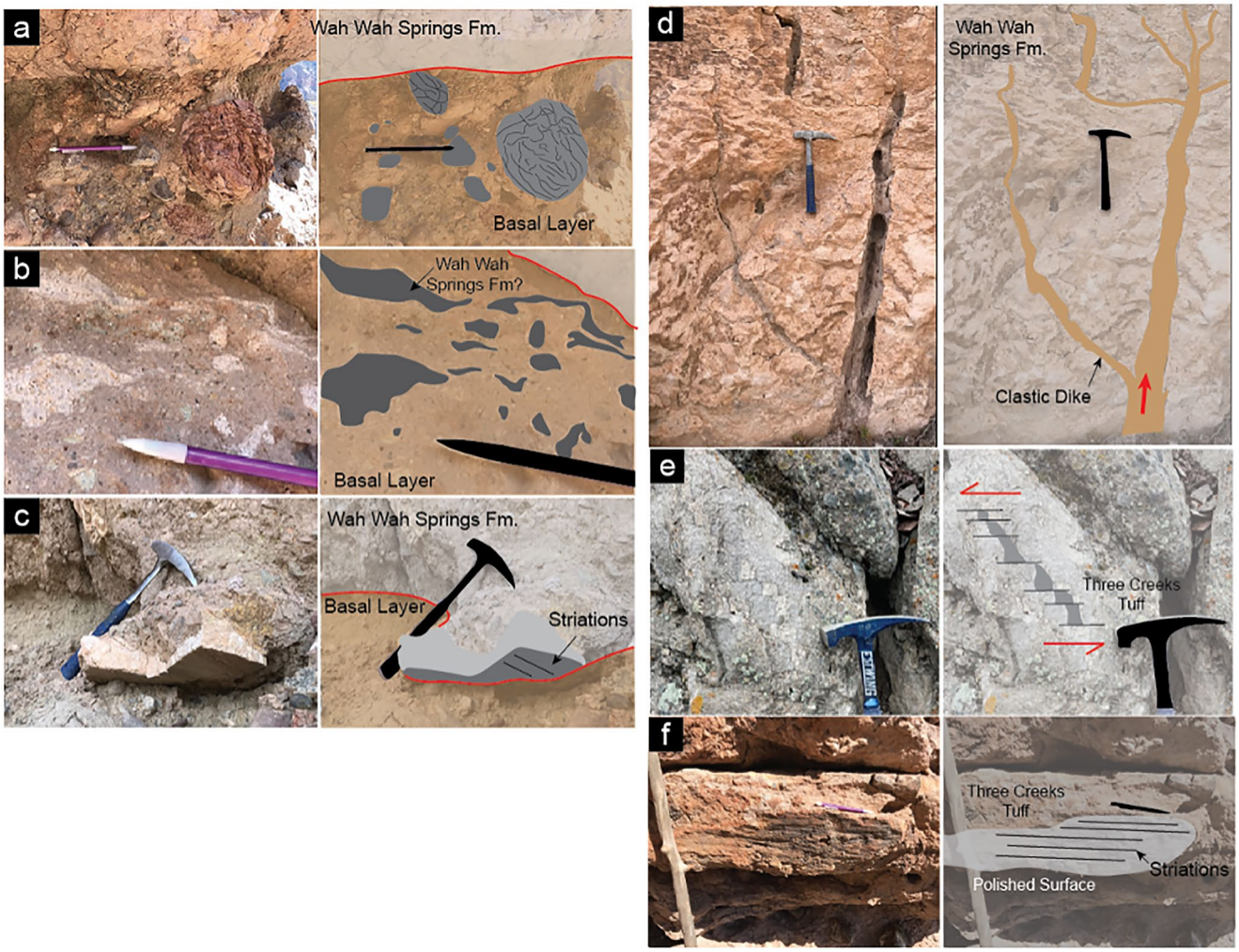

Figure 8. Sevier gravity slide deformation at North Sanford Valley. (a) Pervasively fractured clasts within the basal layer (b) Color banding in the basal layer produced by stretched and contorted volcanic clasts. (c) Cobbles at the basal surface are cut and striated during Sevier gravity slide (SGS) emplacement. (d) Clastic dikes propagate upwards from the basal layer into deformed Wah Wah Springs Formation. (e) Shear fabrics in the Wah Wah Springs Formation display top toward the south displacement, consistent with SGS emplacement. (f) Subvertical fault surfaces with subhorizontal striations consistent with SGS emplacement direction in the Wah Wah Springs Formation.

(Figure 8f). In thin section, the Wah Wah Springs Formation in this portion of the slide contains abundant plagioclase, biotite, and minor quartz that display varying degrees of deformation (Figure 10). Particularly in the upper portion of the thin section, most grains are euhedral in shape and softer, less resistant minerals such as biotite retain original blade like crystal habit (Figure 10b). Other grains show intense damage (Figure 10), with individual mineral grains of quartz and biotite fractured below the grain scale (Figures 10c–10h), and jigsaw textures in which fragments are not significantly rotated (Figures 10c and 10i). Similarly, grains of plagioclase show deformation twinning textures (Figure 10g). Throughout the thin section, bands of comminuted granular material similar in composition to the basal layer material are observed cutting through the section (Figures 10d and 10e). Fractures in crystal grains near these bands are filled with the same granular material.

Above the upper decollement, subhorizontal Kingston Canyon Tuff and Mount Dutton Formation overlie tilted Wah Wah Springs Formation (Figures 6, 11a, and 11c), separated by a thin zone of white to greenish gray granular material (Figure 11b). In contrast to the granular material forming the basal layer along the lower decollement, this material is darker in color, contains fragments of only rock units adjacent to the slide plane, and lacks the diverse mixture of rounded to subrounded volcanic and quartzite cobbles to pebbles. Green to white clastic dikes intrude upwards and downwards from this horizon into the highly weathered and damaged basal vitrophyre of the Kingston Canyon Tuff (Figure 11b). Most clastic dikes are subvertical or slightly curved, though in some

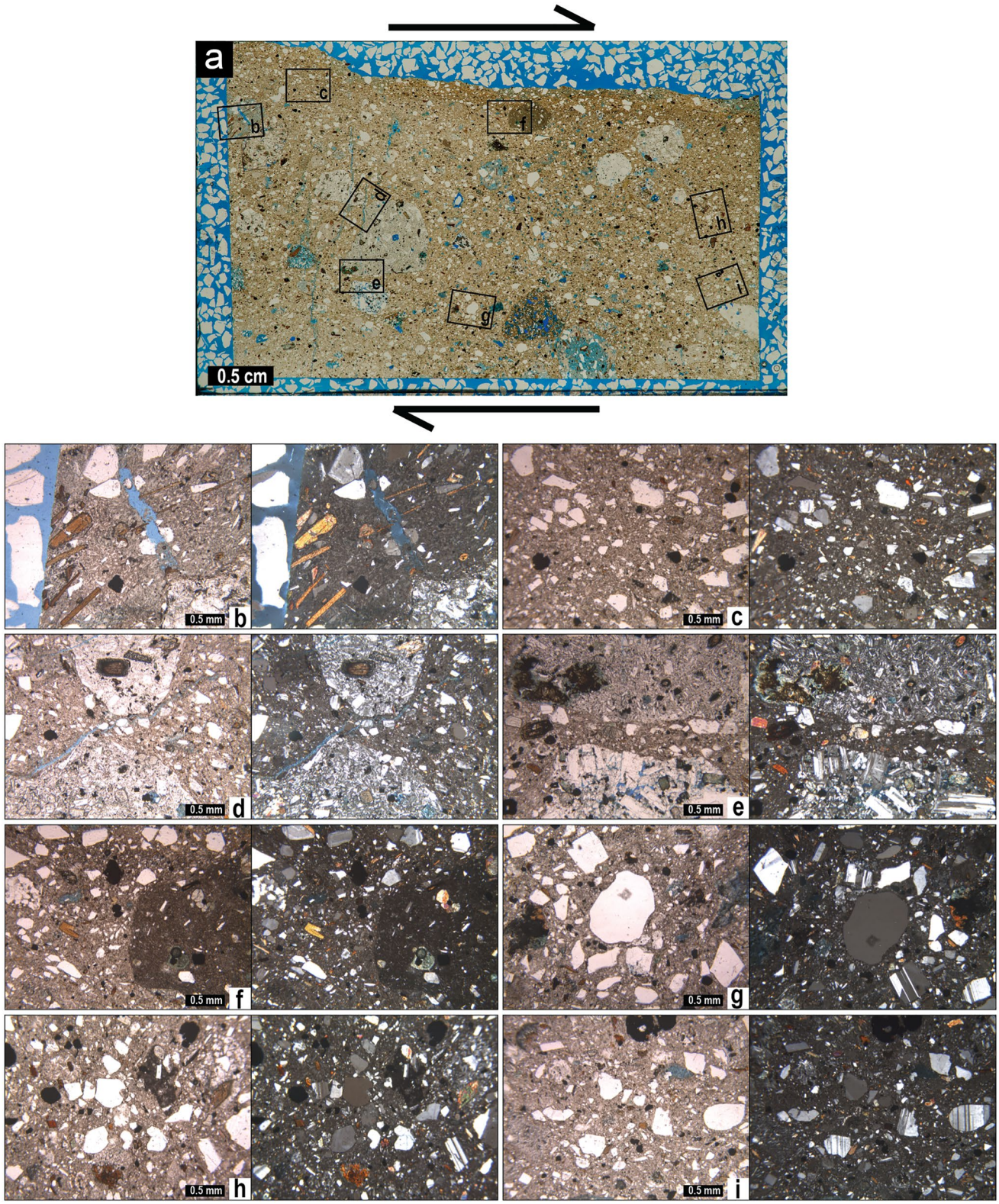

Figure 9. Microstructural observations of basal layer collected from North Sanford Valley. (a) Full slide scan in plane polarized light, with arrows indicating sense of shear. (b) Biotite grains retain rectangular habit in the basal material. Also looks like preferred orientation of biotite. (c) Representative image of mineral grains contained within the basal material. (d, e) Finer-grained material fills the space between rounded larger igneous clasts of Wah Wah Springs Formation. (f) Crude inverse grading of mineral fragments from the boundaries of large igneous clasts. (g, h, i) Additional representative images of crystal fragments in the basal material used to calculate mass dimension. For higher magnification images, the left photo is in plane polarized light, and the images on the right are in cross-polarized light.

10.1029/2022GC010783

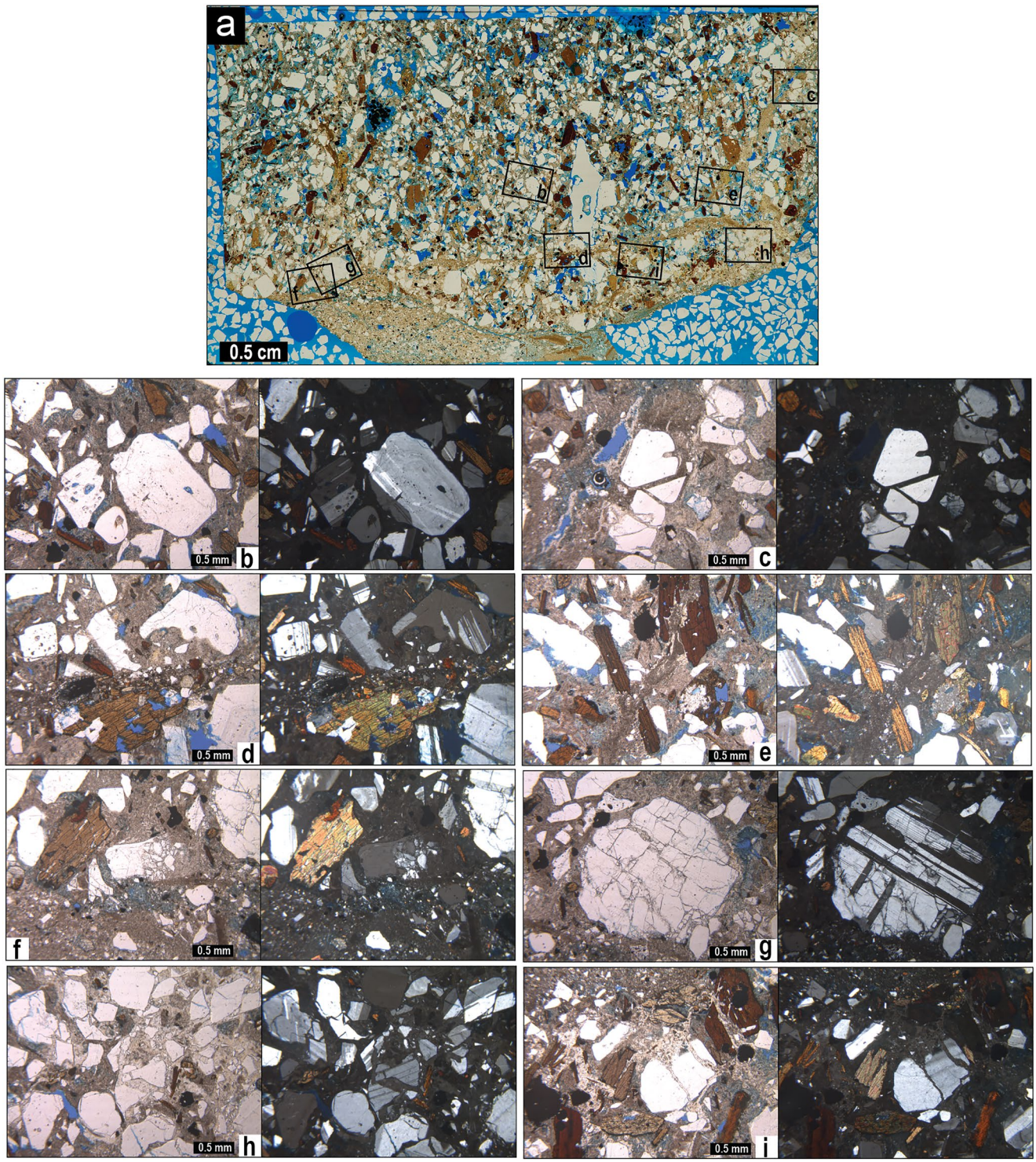

Figure 10. Microstructural observations of allochthonous Wah Wah Springs Formation collected from the central exposures of North Sanford Creek. (a) Full slide scan in plane polarized light. Note the sample is right way up but otherwise unoriented. (b) Representative mineralogy of the Wah Wah Springs Formation showing little grain scale damage. (c) Broken fragments of a quartz grain show low shear strain, common of jigsaw fractures. (d, e) Bands of comminuted material cut across the lower portion of the thin section, split biotite grains, and contain fragments of broken mineral grains adjacent to the band. (f) Shattered quartz grain. (g) Plagioclase grains show deformation twinning textures. (h, i) Additional representative images used to calculate mass dimension. For higher magnification images, the left photo is in plane polarized light, while the images on the right are in cross-polarized light.

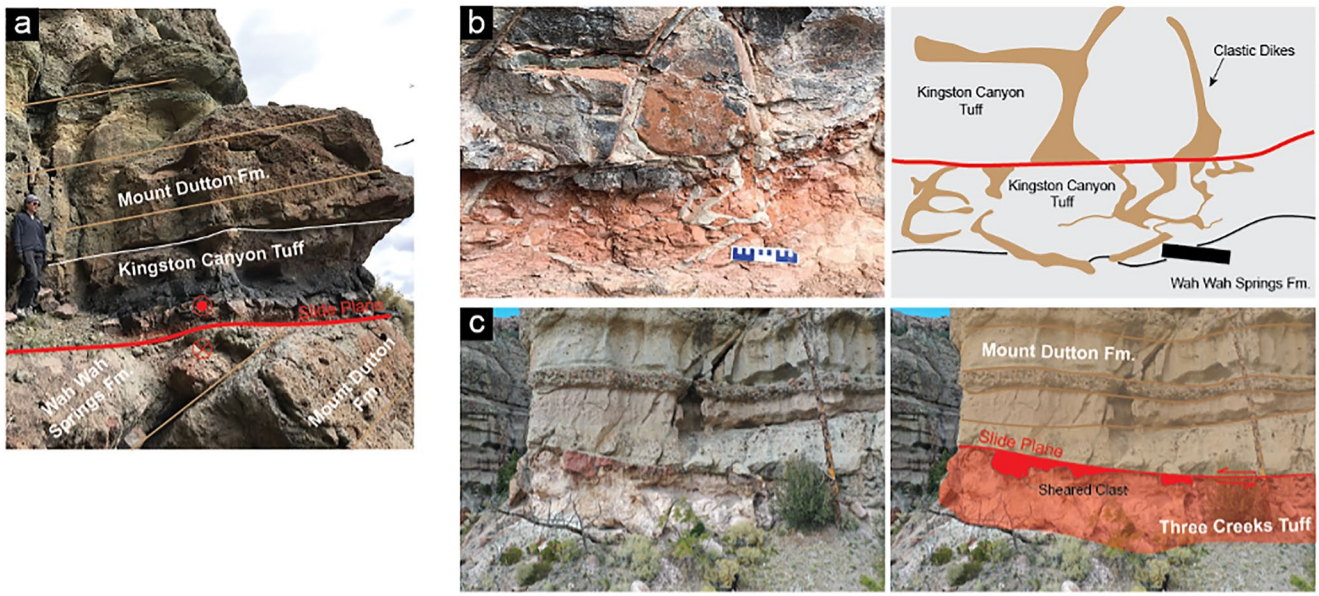

Figure 11. Field photographs of the upper slide surface exposed in North Sanford Valley. (a) Subhorizontal Kingston Canyon Tuff and Mount Dutton Formation overlie north dipping Wah Wah Springs Formation and Mount Dutton Formation. (b) Clastic dikes propagate up and down from a slide horizon within the Kingston Canyon Tuff. (c) The contact is marked by local clasts that appear to be sheared through at the slide surface.

exposures the dikes form a more chaotic network (Figure 11b). Above this horizon contained within the Kingston Canyon Tuff, the Mount Dutton mudflows are intact, with little to no discernible damage and clearly defined, gently west-dipping bedding planes (Figures 6 and 11a).

4.4. Showalter Creek

Showalter Creek (37.813°, −112.225°) is the southernmost exposure of this study and represents some of the most distally transported material preserved in the SGS. Most of the volcanic section, including the Wah Wah Springs Formation, Three Creeks Tuff, and Kingston Canyon Tuff, is missing in the 70 m thick allochthonous blocks at Showalter Creek, and Mount Dutton Formation is separated from autochthonous Brian Head Formation by an up to 25 m thick layer of basal material (Figure 12a). Like North Sanford Valley, the basal slide surface displays significant relief along the exposure, but its general orientation is 255°/19° NW with striations that trend downdip between 001° and 006° (Figure 13). Unlike sites to the north, the uppermost ~30 m of the Brian Head Formation is folded and faulted along shallow, small-displacement faults (Figures 12b and 12c). These faults strike east-west with dips of approximately 30° to 40° to the north and south (Figure 13) and reverse-sense displacement. Kinematic indicators were not observed on slip surfaces, but assuming near dip-slip displacement, these faults are consistent with north-south directed shortening (subparallel to striations on the basal contact) and thickening in the vertical direction (Figure 13). Brian Head strata below this zone are undeformed and subhorizontal (Figure 12a).

The basal layer at Showalter Creek contains deformed and strained clasts of likely Three Creeks Tuff (Figure 12d) that are oriented subparallel to the basal surface, as well as abundant clasts derived from the Brian Head Formation (Figures 12e, 14c, and 14d). Color banding is also present in the basal layer and subparallel to the basal slide plane (Figure 12f). Thin sections of the basal layer collected at Showalter Creek show matrix-supported material with clasts up to 1 cm in diameter (Figures 14a–14f). Clasts are generally smaller than 1 mm in diameter and sedimentary clasts derived from the Brian Head Formation are more abundant than igneous clasts (Figures 14a–14f). Some clasts of Wah Wah Springs Formation and Kingston Canyon Tuff are present (Figure 14e). Quartz grains are more abundant than plagioclase (Figures 14a–14e) and biotite only occurs in smaller fragments (Figures 14b and 14d) than observed in basal material from Cottonwood Creek and North Sanford Valley. Both clasts and crystal fragments are subrounded, intact, and show no clear preferred orientation or discernible fabric to the matrix (Figure 14)

Upper plate Mount Dutton lava and mudflows are deformed through the entire ~40 m thickness of the exposure and bedding is difficult to discern with certainty (Figure 12). Near the slide base, thrust faults cut upwards from

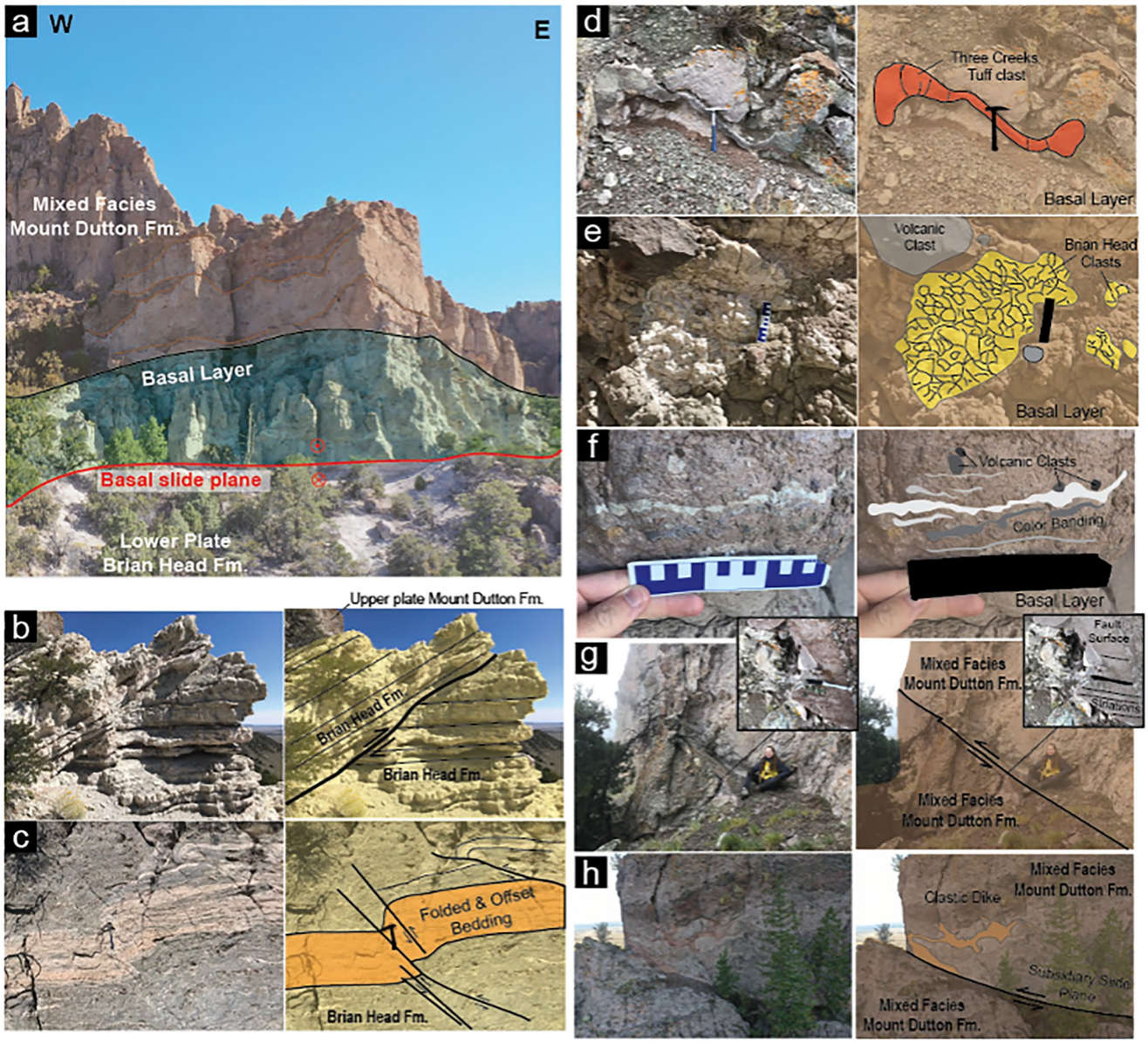

Figure 12. Sevier gravity slide deformation at Showalter Creek. (a) Outcrop scale map of the allochthonous Mount Dutton Formation overlying Brian Head Formation, separated by a 25 m thick basal layer. (b) Shallow thrust faulting in the uppermost Brian Head Formation. (c) Thrust fault and folding in the Brian Head Formation. (d) Clasts of Three Creeks Tuff in the basal layer are cataclastically deformed, stretched, and thinned. (e) Rip up clasts of substrate Brian Head Formation are intensely fractured. (f) Crude color banding in the Showalter Creek basal layer. (g) Internal faulting within the Mount Dutton Formation. (h) Clastic dikes propagate upwards from a sliding surface within the Mount Dutton Formation.

the basal slide plane through the Mount Dutton Formation (Figure 12g), resulting in northward tilting. Furthermore, UAV imagery in the cliff face of a surface subparallel to the basal slide plane from which clastic dikes propagate upwards (Figure 12h) suggests the presence of multiple slip surfaces.

5. Discussion

5.1. Evidence of Rapid Upper Plate Emplacement

The formation of glassy pseudotachylyte at Cottonwood Creek (Figure 5f) and along subsidiary slip surfaces throughout the upper plate of the SGS provide evidence for high velocity sliding during emplacement. We interpret these features to be frictional melts following the mesoscale criteria defined by Magloughlin and Spray (1992), including a glassy texture with quenched margins at the contact with host rock and the occurrence of vesicles

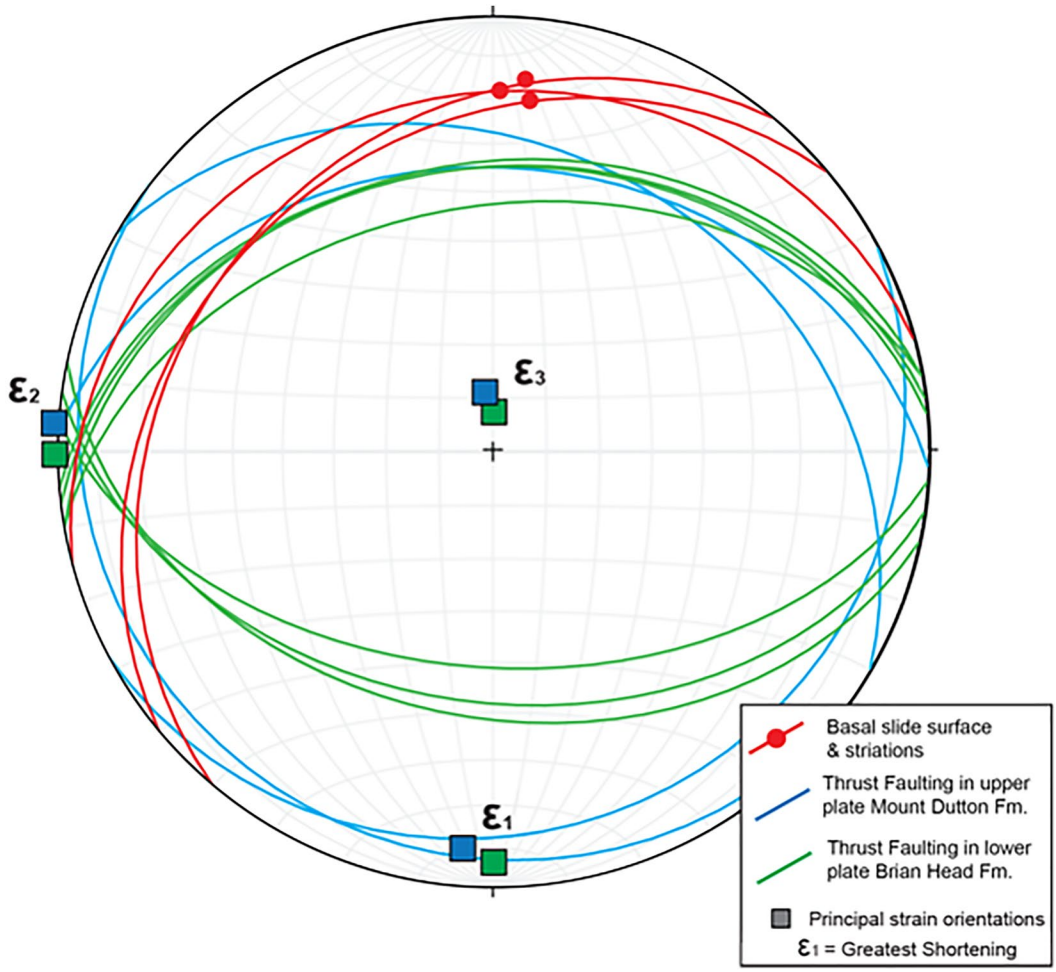

Figure 13. Equal area stereographic projection of slip surfaces and internal deformation observed at Showalter Creek. The basal surface of upper plate blocks is north dipping with striations consistent with southward transport. Slip surfaces in the upper plate (blue) and lower plate (green) are dipping toward the north and south steeper than the basal slide surface. Kinematic inversions are color coded for upper and lower plate data and calculated assuming pure dip slip.

and embayed clasts contained within the glass (Figure 5f). Similar features studied in more detail on the adjacent Markagunt gravity slide also show glassy textures, quenched vein margins, and vesicles and amygdule fillings at the mesoscale, and survivor quartz grains within an isotropic groundmass, flow banding, and microlites in thin section (Biek et al., 2019; Hacker et al., 2014; Holliday et al., 2022; Zamanialavijeh et al., 2021).

Pseudotachylyte genesis requires frictional heating during slip to increase the temperature beyond the melting temperature of some mineral constituent in the surrounding rock mass by frictional heating (Masch et al., 1985; Spray, 1995). When observed in the rock record, it is generally attributed to high sliding velocities associated with processes of earthquake rupture (Rowe et al., 2012; Rowe & Griffith, 2015) and impact structures (Thompson & Spray, 1996). Pseudotachylyte formed during landslide emplacement is rare with a few examples noted globally, including glass shards observed in the Heart Mountain carbonate basal layer (Craddock et al., 2009) and as veins along the basal surface of the Köfels Slide of Austria (Masch et al., 1985) and the Arequipa Slide in Peru (Legros et al., 2000). In landslides, frictional heating resulting in pseudotachylyte formation requires thick packages of slide material, high-velocity sliding, and high frictional contact across the slip surface (Legros et al., 2000). We have not identified any pseudotachylyte along the basal slip surface of the SGS, and pseudotachylyte glass is observed only along stratigraphically higher subsidiary slip surfaces and as injection veins in the allochthonous material within the upper plate (Biek et al., 2019). This suggests differences in the frictional strength between the stratigraphically higher slip surfaces where frictional heating resulted in the generation of a melt phase, in contrast to the basal slide surface that did not achieve temperatures high enough to form a melt.

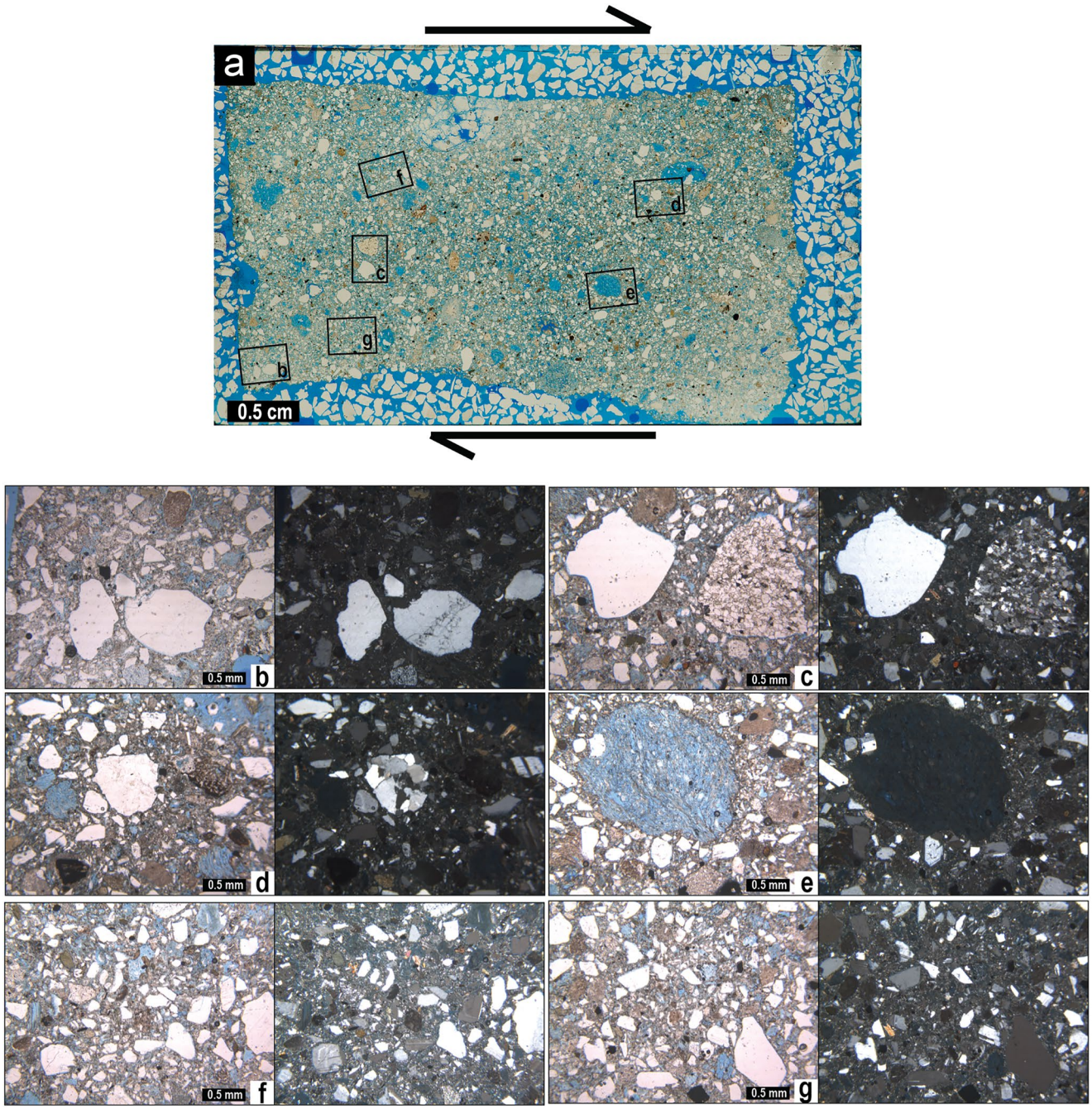

Figure 14. Microstructural observations of basal layer collected from Showalter Creek. (a) Full slide scan in plane polarized light, with arrows indicating sense of shear. (b) Representative image of basal material, primarily containing angular to subrounded grains of quartz. (c, d) Subrounded sedimentary clasts of quartz are interpreted as derived from the Brian Head Formation are common in the basal material. (e) Subrounded clast of Kingston Canyon Tuff. (f, g) Additional representative images of mineral fragments in the basal material used to calculate mass dimension. For higher magnification images, the left photo is in plane polarized light, and the images on the right are in cross-polarized light.

5.2. Spatial Variation in Gravity Slide Structure

5.2.1. Upper and Lower Plate Structure

Along the slide transport parallel profile, the SGS upper plate consists of numerous mountain-sized blocks of intact volcanic rocks with boundaries defined by variations in stratigraphy, bedding attitude, structures, and overall damage state. Broadly, the upper plate displays a high degree of internal coherency that preserves the

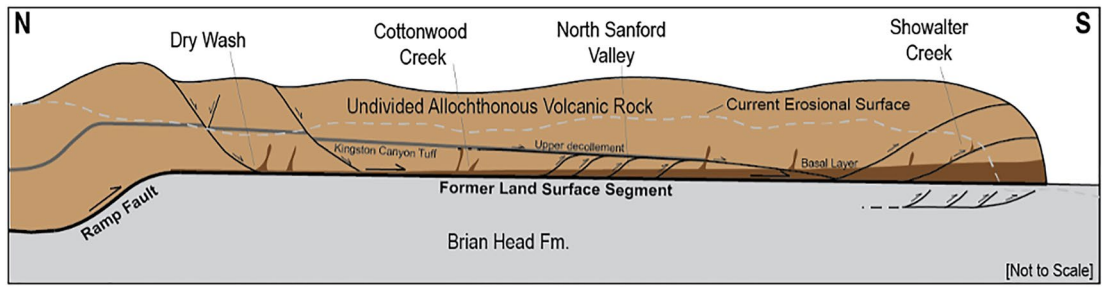

Figure 15. Schematic illustration of the spatial distribution of damage styles and deformation structures observed at the four sites described as a function of distance south of the ramp of the Sevier gravity slide. Deformation in the north is primarily extensional, whereas sites toward the distal portion of the slide display more heterogeneous deformation including horizontal shortening. The basal vitrophyre of the Kingston Canyon Tuff is not observed south of the North Sanford Valley site. South of this site the basal layer (dark brown) thickens progressively toward the slide terminus.

original and upright, though attenuated and damaged, stratigraphic succession like megabreccias described in smaller volcanic landslides (e.g., Legros et al., 2000; Pollet & Schneider, 2004; Schneider & Fisher, 1998; Shaller et al., 2020). Near the basal contact, the upper plate is intensely fractured into rock and crystal fragments by jigsaw fractures and along anastomosing shear fractures (Figures 4a, 5e and 10). In the SGS, brecciation is most apparent in the ash flow tuffs compared to mudflow deposits in which only some clasts display jigsaw fracturing, but all sites display an overall general decrease in damage state with increasing vertical distance above the basal surface. This is most apparent in the transition from mixed facies in the allochthonous plate at the basal surface to the undisturbed block facies observed at Cottonwood Creek (Figure 5a). Portions of the upper plate that experienced greater translation distance across the former land surface, such as Showalter Creek, also display thicker damage zones. At Dry Wash and Cottonwood Creek, the mixed facies zone extends <10 m above the basal surface (Figures 4a and 5a), while mixed facies deformation characterizes nearly the entire ~ 60 m thick exposure of allochthonous rock at Showalter Creek (Figure 12a). In addition to the thickness of the damaged mixed facies zone, slide blocks that experienced greater translation across the former land surface also display evidence of greater mechanical wear and extensional deformation by thinning of the allochthonous plate. Slide blocks to the north such as Cottonwood Creek preserve the most complete volcanic section in the SGS (Figure 3), including major ash flow tuffs of the Wah Wah Springs, Three Creeks, and Kingston Canyon (Figure 5a). Closer to the slide terminus at Showalter Creek, these ash flow tuffs are missing, and stratigraphically higher Mount Dutton Formation is the principal upper plate unit (Figure 12a).

Larger-scale internal deformation structures formed during SGS emplacement vary as a function of distance south of the ramp (Figure 15). At the northern Dry Wash and Cottonwood Creek sites, damage styles in the upper plate are most consistent with simple translational deformation focused near the basal slide surface. Slip appears to be limited to the lower portion of the slide and thinning and stretching of slide material (Figure 4d) suggests primarily extensional deformation. Generally, little to no deformation is observed in the lower plate at these sites and autochthonous bedding surfaces remain subhorizontal. To the south of the North Sanford Valley site, deformation structures in the slide mass are more varied and both strike slip and horizontal compressional style faulting are observed. Similarly, at Showalter Creek near the slide terminus, the upper plate Mount Dutton Formation shows evidence of multiple slide surfaces through the slide block (Figure 12h) and steeply dipping internal reverse faults (Figure 12g). At Showalter Creek, the uppermost Brian Head Formation in the lower plate is deformed, with shallow south vergent fold and thrust deformation immediately below the basal slide plane (Figures 12b and 12c).

5.2.2. Basal Layer

The SGS basal layer at all sites is a matrix-supported, poorly sorted sandstone to conglomerate that contains material derived from frictional wear processes during emplacement; it resembles granular material described beneath large slide masses (Anders et al., 2000; Dufresne et al., 2021; Malone et al., 2014; Mayback et al., 2022; Weidinger et al., 2014; Yarnold & Lombard, 1989). Macroscopically, the texture of basal material does not vary significantly; however, clast and mineral fragment composition changes with position south of the ramp, suggesting changes in the upper and lower plate rock units that are exposed to frictional wear during emplacement. At the northern sites of Dry Wash and Cottonwood Creek, wear products in the basal layer are primarily volcanic,

with abundant igneous clasts and free quartz, plagioclase, and biotite mineral fragments. Clasts of the underlying Brian Head Formation are not abundant in the basal layer until farther to the south, where greater proportions of quartz and rounded to subangular clasts of quartz-rich sandstone occur. At Showalter Creek, intensely fractured rip-up Brian Head clasts (Figure 12e) are more abundant than igneous clasts, and volcanic minerals such as biotite and plagioclase are rarer and smaller in size than those observed to the north. Some clasts of tuff are intensely fractured and sheared at Showalter Creek (Figure 12d), while others remain subrounded and largely undamaged (Figures 14a and 14e).

Across the runout portion of the SGS across the former land surface segment, the thickness of the basal layer increases with distance south of the ramp. At Dry Wash and Cottonwood Creek, the thickness of the basal layer is less than 1 m, but it increases near the southern terminus of the slide, exceeding 25 m at Showalter Creek. Basal material intruding into rocks immediately adjacent to the basal zone is a ubiquitous feature throughout the deposit, and there is no particular site or portion of the slide in which these features occur more frequently than others. Clastic dikes vary in size from tens of meters in length to <1 m and propagate both upwards into the allochthonous blocks and, less frequently, downwards into lower plate Brian Head Formation. These features form by forceful injection of basal material and suggest high fluidity and the presence of elevated fluid pressures at the base of the slide when formed (Jolly & Lonergan, 2002). Similar injection features were described by Legros et al. (2000) and Johnson (1978) at smaller landslides and by Malone (1995) and Craddock et al. (2012) for the Heart Mountain slide.

5.3. Implications of Structural Variation

5.3.1. Deformation of the Upper Plate

For much of the runout portion of large landslides, deformation styles are extensional and translational (Schneider & Fisher, 1998; Weidinger et al., 2014), consistent with those across the northern portions of the SGS former land surface segment. In the transport-parallel exposures at Dry Wash, we observe significant thinning and extensional deformation of the allochthonous block in the form of pinch and swell geometries between lithologies and boudinage-like structures within the mixed facies zone (Figures 4a and 4d). Further complexity in the observed deformation, such as the internal thrust faulting observed at North Sanford Valley and Showalter Creek, suggests a change in the kinematics of internal deformation within the upper plate during emplacement. Kinematic inversions of these structures (shown in Figures 7 and 13) suggest the principal shortening direction is oriented subhorizontal toward the south (plunging 2° toward 180 to 190°), resulting in thickening in the vertical direction. The calculated shortening directions obtained from these inversions are generally consistent with the translation direction of the slide measured directly from striations on the basal surface (Figures 7 and 13), supporting our hypothesis that the features formed during SGS emplacement.

Previous studies of large-volume landslides, such as the Blackhawk landslide of California and Heart Mountain slide, report similar imbricate structures, which are attributed to zones of abrupt deceleration that propagate rearward as momentum carries trailing material overtop a decelerating slide front (Johnson, 1978; Shreve, 1968). This mechanism can account for the internal thrust faulting and formation of secondary, stratigraphically higher slip surfaces within the mixed facies of the Mount Dutton Formation near the distal end of the slide at Showalter Creek (Figure 12g) during deceleration of the slide. Internal compressional deformation in more central portions of the SGS, such as the North Sanford Valley, may similarly reflect zones of rapid deceleration. Potential causes of the rapid deceleration of the North Sanford Valley upper plate include collision and interaction between individual slide blocks or against pre-existing topography on the former land surface. The material at the southern end of the imbricate thrust structure observed in North Sanford Valley (Figure 6) is too damaged to definitively distinguish between these two possible causes. Compressional deformation results from rapid deceleration of the leading edge of the slide, further breakdown of the upper plate due to strain partitioning and dynamic disintegration, and rearrangement of transport direction around an obstacle (Figures 6 and 8f). In the North Sanford Valley site, we interpret the upper and lower decollements to be coeval due to the consistency of kinematic indicators between the two slip surfaces and the general immaturity of the wear products formed along the upper decollement. Unlike the lower decollement basal material that incorporates cobbles rounded by fluvial processes on the former land surface prior to slide emplacement, the upper decollement material does not show any evidence of being exposed to erosional and depositional processes between two failure events. Additionally, the stratigraphic position of the slip surface remains constant toward the north and we do not observe any evidence, such as repeating stratigraphic sections, that would suggest overlapping retrogressive failures.

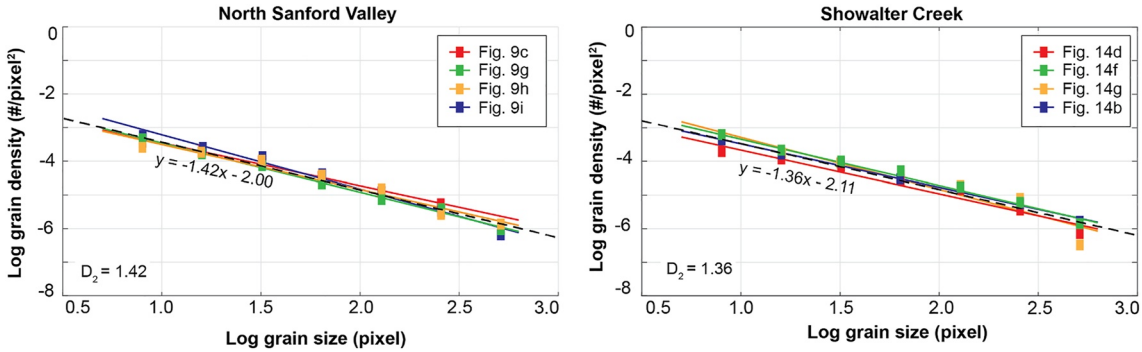

Figure 16. Grain size distribution plots from the basal layer collected from North Sanford Valley (left) and Showalter Creek (right). Mass dimensions (D_2) are consistent between the two sites, and generally lower than values obtained in highly sheared fault rocks. Images used in analysis were captured at 25x magnification with 655 pixel/mm.

5.3.2. Frictional Wear

The relationship between grain size and spatial density of each binned grain size (Figure 16) within the observation window of basal material samples is well fit by a power law relationship, suggesting formation by mechanical wear processes originating from fault-style constrained comminution resulting from shear strain across the granular basal zone (Frost et al., 2009; Sammis & King, 2007). Previous studies in fault zones demonstrate the fractal dimension D_2 increases toward localized zones of shear, with $D_2 = 0.88$ observed in fault rocks collected at the periphery of major fault zones and material collected from the strongly foliated fault core rock yielding $D_2 = 2.0$ (Billi et al., 2003; Billi & Storti, 2004; Chester et al., 2005). Multiple analyses of basal material collected from the North Sanford Valley and Showalter Creek sites yield a mass dimension ranging between 1.32 and 1.46 (Figure 16), which is consistent with or just below values typical of gouged and brecciated rock outside fault cores in well-developed faults (e.g., Anderson et al., 1983; Billi & Storti, 2004; Chester et al., 2005; Sammis et al., 1987). These values are extremely low if translation distances of ~30 km accommodated primarily within this zone. As the D_2 obtained for the basal material of the SGS is consistent between the two sites and generally lower than expected for processes of constrained comminution in long lived fault zones (e.g., Sammis & King, 2007), we suggest the SGS basal layer represents an immature shear zone. This is also consistent with observations of poor mixing across large areas and varying sources of wear products with translation distance described above, collectively indicating continual deposition of wear products at the base of the slide and renewal of the slip surface during emplacement.

In comparison, D_2 obtained for allochthonous Wah Wah Springs Formation collected at North Sanford Valley (Figure 10) range between 0.74 and 1.24 depending on the location within the thin section and overall damage state. Images captured from zones of deformation yield mass dimension values at the higher end of this range, reflecting greater mechanical breakdown of individual quartz and feldspar and fewer large grains. Images captured in less clearly deformed portions of the thin section yield lower values that are more consistent with those observed at the periphery of major fault zones (Frost et al., 2009). At the higher end of D_2 observed in allochthonous material from North Sanford Valley, the particle size distribution of the damaged Wah Wah Springs Formation closely reflects those observed in both basal layer samples, suggesting a similar grain size distribution. During slide emplacement, we hypothesize that frictional wear and grain breakdown are most concentrated in the lowermost portion of the upper plate, forming individual mineral fragments that are incorporated into the basal layer as the lowermost slide material disaggregates. Once incorporated into the basal layer, the mass dimension suggests that grain size does not dramatically change from that of damaged allochthonous material, indicating that the basal material does not experience significantly more breakdown and reworking between incorporation and deposition. We interpret rounded igneous clasts in the basal layer to have been incorporated from unconsolidated material on the former land surface and worn by erosional processes prior to initiation of the SGS due to the overall lack of damage observed in most large basal material clasts, though additional wear likely occurred by mechanical abrasion during shear.

The increasing thickness of the basal layer with translation distance across the former land surface (Figure 15) indicates an increase in the rate of wear and breakdown of the upper allochthonous plate and preservation of wear

products with translation distance, as more material is generated by mechanical breakdown of the upper plate and deposited at the base of the slide. The rate of wear product generation reflects several processes, including the increase in overall damage state of slide blocks with greater transport across the land surface, exposure of less resistant Mount Dutton Formation at the basal slide surface after breakdown, and loss of the more resistant ash flow tuff units, and an increase in frictional contact between the upper and lower plates as slide blocks slow. The thick basal layer at Showalter Creek (Figure 12a) may also reflect contributions from a bulldozing effect near the leading edge of the slide (Shreve, 1968). Larger-scale deformation suggests this may be in part due to increased frictional coupling between the upper and lower plate, suggesting mechanisms that reduce frictional resistance and promote sliding became less efficient toward the distal end of the slide. In the proximal area of the slide at Dry Creek near the ramp fault, the lack of deformation of lower plate rocks suggests little frictional contact of the upper plate during emplacement. This is also consistent with mineral fragments preserved in the basal layer that are derived primarily from the upper plate volcanic rocks. Further to the south at Showalter Creek, evidence of strong frictional contact becomes more apparent. Incorporation and accretion of substrate material in the form of rip up Brian Head clasts and large blocks, and of unconsolidated material from the former land surface, suggests local scour, and unlike at sites to the north, shallow folding and thrusting in autochthonous Brian Head Formation below the slide plane suggests significant frictional coupling as the slide overrode this portion of the former land surface.

5.3.3. Slip Localization

Properties of the basal deformation zone indicate slip was primarily accommodated within the narrow basal layer, which ranges in thickness from ~0.5 m at the northern Dry Wash site to >25 m at the distal Showalter Creek site. However, some exposures show evidence for more distributed shear. Shear features with top to the south displacement observed above the basal layer (Figure 8e) suggest distributed deformation extended into the mixed facies zone of the upper plate at North Sanford Valley and overall damage states suggest reworking of this material. The presence of pseudotachylyte within the upper plate also suggests the formation of secondary slip surfaces and more distributed shear within the slide mass. Considering the thickness of both the basal layer and mixed facies along a transport-parallel profile, the thickness of the available zone to accommodate slip at the base of the slide increases dramatically in the direction of slide movement, resulting in overall greater degrees of slip delocalization between the upper and lower plates.

We also observe stratigraphically higher zones of localized shear that accommodated slip along planes of pre-existing weakness such as lithologic boundaries in slide blocks. In some cases, these are preserved tens of meters above the mixed facies zone and are evident by frictional melting and the formation of pseudotachylyte (Figure 5f) and clastic dikes (Figures 11b and 12h). Similar to the distributed deformation in the lower plate Brian Head Formation observed at Showalter Creek, we believe that these stratigraphically higher slip surfaces formed during the late stages of emplacement. As frictional contact at the base of the slide increased and resulted in slowing of the lowermost portion of the slide block, the momentum of the upper portions may have resulted in internal shearing and the formation of new slip surfaces along preferred surfaces of weakness such as bedding planes (e.g., Pollet & Schneider, 2004).

5.4. Mechanisms of Sliding and Cessation

Based on these observations, we develop a conceptual model for the emplacement of the SGS. Magma intrusion and rapid inflation of the volcanic field during late-stage activity (Hacker et al., 2014) and an evolving regional stress regime (Hoiland et al., 2022) may have contributed to gravitational instability and collapse of the southern MVF, resulting in the initiation of the SGS. During the earliest stages of initiation and throughout the translation history, the upper plate is modified and broken down by retrogressive failure in the breakaway region and by dynamic disintegration processes and strike-parallel segmentation along internal faults (Boyer & Hossack, 1992; Pollet & Schneider, 2004). Variations in striation orientation suggest rearrangement of transport direction and rotation of blocks during sliding, potentially by interaction with various blocks or around pre-existing topography.

Characteristics of the basal layer underlying the Sevier gravity slide, including abundant clastic dikes and grading and flow banding of coarse intervals, suggest that the material was highly mobile or fluidized during slide emplacement and provided the low shear strength environment needed to buffer the autochthonous Brian Head Formation from extensive deformation. While dry granular materials can become fluidized by mechanical

processes (e.g., Anders et al., 2000; Campbell et al., 1995; Melosh, 1979), fluidization during the emplacement of long-runout landslides may be easier to achieve with the presence of pressurized water or gases (e.g., Anders et al., 2010). In the SGS basal layer, the lack of severely deformed grains observed in the thin section (Figures 9 and 14) and fine-grained matrix suggests the high energy elastic collisions of grains were infrequent during sliding and likely unable to result in mechanical fluidization. Unlike the Heart Mountain slide, where carbonates of the Big Horn Dolomite could provide carbon dioxide into the basal layer during thermal decomposition resulting in gas fluidization (e.g., Anders et al., 2010), there are no clear lithologic sources of such gases within the Sevier gravity slide upper or lower plates.

During frictional slip, localized heating in the shear zone can result in thermal pressurization of pore fluids when volumetric expansion of fluids exceeds that which can be accommodated by compression of the surrounding rock (Lachenbruch, 1980; Mase & Smith, 1985; Rice, 2006). Thermal pressurization is ubiquitous in earthquakes (Viesca & Garagash, 2015), and given that it is not strictly limited to a single lithology, the mechanism might be similarly important in long-runout landslides. The mechanisms of carbonate decomposition and pressurization suggested for the emplacement of the Heart Mountain Detachment are in contrast lithology-dependent (Goren et al., 2010; Mitchell et al., 2015). Thermal pressurization was previously proposed as a possible mechanism for the apparent low frictional resistance of large-volume landslides (e.g., Goren & Aharonov, 2007; Vardoulakis, 2002) and the abundance of clastic dikes throughout the SGS suggests that elevated fluid pressures likely contributed to the apparent low frictional resistance during emplacement. The presence of well-developed and far reaching clastic dikes that formed upstream of the site containing cm scale clasts just to the south of the ramp at Dry Wash indicates that elevated fluid pressures developed early in the slide history within the breakaway segment of the slide.

Portions of the allochthonous plate with short translation distances across the former land surface preserve the record of highly effective dynamic weakening mechanisms, high basal fluid pressures and fluidization of the basal layer material and low frictional contact with the underlying substrate during emplacement. Exposures of the basal zone at Dry Wash and Cottonwood Creek reveal thin zones of deformation representing high degrees of slip localization and internal damage limited to thin regions immediately overlying the basal zone. The complete volcanic section at these sites, including the highly impermeable ash flow tuffs and basal vitrophyre of the Kingston Canyon Tuff, likely promoted the maintenance of elevated fluid pressures over great sliding distances. Steady state flow tests of these units provide a permeability of $\sim 10^{-21}$ m^2 (Braunagel et al., 2021), suggesting that they can effectively create undrained conditions and slow the rate of pressure diffusion outside the basal and mixed facies zones. During emplacement, elevated fluid pressures generated by frictional heating and thermal expansion would have effectively been trapped in the basal zone by the undrained conditions created by these tuff units, reducing the frictional contact between the slide mass and substrate and limiting deformation to a narrow zone above the basal plane. Across the runout portion of the Sevier gravity slide, incorporation of unconsolidated saturated material from the former land surface and uppermost lower plate Brian Head Formation, along with continued exposure of fresh upper plate rock along the wear surface, may have provided the mechanism needed to recharge increasing volumes of water into the basal zone.

South of Cottonwood Creek, impermeable ash flow tuff units are no longer preserved within the slide mass, presumably lost to frictional wear and incorporation into the basal layer, leaving the stratigraphically higher Mount Dutton Formation immediately overlying the basal zone. Unlike the welded ash flow tuffs, the permeability of the Mount Dutton Formation is much higher, with steady state flow test results on intact samples yielding values between 10^{-18} and 10^{-12} m^2 (Braunagel et al., 2021). Additionally, the increasing damage state is also expected to increase the overall permeability of the overriding slide mass. Laboratory testing of damaged samples indicates that fracture damage increases permeability by up to six orders of magnitude (e.g., Aben et al., 2020; Jiang et al., 2010). Due to the increasing permeability with slip distance owing to the loss of volcanic units near the basal zone and the overall increase in damage state, the diffusion rate of elevated fluid pressures outside the basal zone increases dramatically, reducing the effectiveness of the thermal pressurization mechanism. The disturbed Mount Dutton Formation observed at Showalter Creek may reflect widespread fluidization of the slide material created by the rapid diffusion of elevated fluid pressures into the overlying slide block. This process is further aided by the increasing rate of mechanical breakdown and deposition of material into the basal layer creating a wider shear zone, more distributed shear, and reducing the rate of heat generation (Lachenbruch, 1980). Collectively, the increasing permeability of overriding slide material and the increasing rate of pressure diffusion out of the basal zone contributed to greater frictional contact, greater rates of mechanical breakdown and

deposition of wear products in the basal zone, and increased slip delocalization, creating a feedback loop that resulted in deceleration of SGS blocks.

As the elevated fluid pressures aiding slip at the leading edge of the damaged slide mass are lost, greater frictional contact promotes deceleration and ultimately cessation of the leading edge of the slide mass. As the leading edge slows, trailing blocks overtake the slide front, resulting in imbricate structures due to the rearward propagation of the deceleration zone (Johnson, 1978; Malone, 1995; Shreve, 1968) and the formation of the steeply dipping reverse faults and stratigraphically higher slip surfaces that are observed at North Sanford Valley and Showalter Creek.

6. Conclusions

The Sevier gravity slide (SGS) records the large-scale gravitational collapse and long-runout translation of the southern flank of the Marysvale volcanic field. In this study, we characterize four exposures of the basal zone of the SGS and document variations in the deformation style and the degree of strain localization as a function of translation distance across the former land surface. Observed deformation styles are consistent with high velocity sliding during the emplacement of the SGS, and clastic dikes and other features indicate that the apparent coefficient of friction during emplacement was reduced by the presence of elevated pressures within a fluidized basal layer. With distance south of the ramp, we observe a transition to slip delocalization within a thickening basal layer, resulting in normal frictional contact and more widespread deformation associated with slide emplacement. This type of deformation, block interaction, and spreading presents a challenge for numerical models of large-scale slide emplacement, which infer a rigid block sliding with no internal deformation and evaluate the efficacy of the model based on the runout distance of the single block.

Data Availability Statement

The 3D structure from motion photogrammetry outcrop models of the four sites described in this study used for outcrop-scale characterization is available at Braunagel (2023).

Acknowledgments

This research was funded by the National Science Foundation under Grants 2113155 to W. A. Griffith, 2113156 to T. Rivera, 2113157 to D. Hacker, 2113158 to D. Malone, and a GSA graduate student research grant to M. Braunagel. We thank Derrick James, Sarah Rose Lesmann, Gracie Stevens, and William Finucane for field assistance. This manuscript was greatly improved thanks to constructive reviews from Mark Anders and an anonymous reviewer.

References

Aben, F. M., Doan, M.-L., & Mitchell, T. M. (2020). Variation of hydraulic properties due to dynamic fracture damage: Implication for fault zones. *Journal of Geophysical Research: Solid Earth*, *125*(4), e2019JB018919. https://doi.org/10.1029/2019JB018919

Aharonov, E., & Anders, M. H. (2006). Hot water: A solution to the Heart Mountain detachment problem? *Geology*, *34*(3), 165–168. https://doi.org/10.1130/G22027.1

Anders, M. H., Aharonov, E., & Walsh, J. J. (2000). Stratified granular media beneath large slide blocks: Implications for mode of emplacement. *Geology*, *28*(11), 971–974. https://doi.org/10.1130/0091-7613(2000)28<971:SGMBLS>2.0.CO;2

Anders, M. H., Fouke, B. W., Zerkle, A. L., Tavarnelli, E., Alvarez, W., & Harlow, G. E. (2010). The role of calcining and basal fluidization in the long runout of carbonate slides: An example from the Heart Mountain Slide Block, Wyoming and Montana, U.S.A. *The Journal of Geology*, *118*(5), 577–712. https://doi.org/10.1086/656383

Anderson, J. J., & Rowley, P. D. (1975). Cenozoic stratigraphy of Southwestern High Plateaus of Utah. In J. J. Anderson, P. D. Rowley, R. J. Fleck, & A. E. M. Nairn (Eds.), *GSA special paper cenozoic geology of southwestern high Plateaus of Utah*. https://doi.org/10.1130/SPE160-p1

Anderson, L., Osbourne, R. H., & Palmer, D. F. (1983). Cataclastic rocks of the San Gabriel fault: An expression of deformation at deeper crustal levels in the San Andreas fault zones. *Tectonophysics*, *98*(3–4), 209–251. https://doi.org/10.1016/0040-1951(83)90296-2

Bemis, S. P., Micklethwaite, S., Turner, D., James, M. R., Akciz, S., Thiele, S. T., & Bangash, H. A. (2014). Ground-based and UAV-based photogrammetry: A multi-scale, high-resolution mapping tool for structural geology and paleoseismology. *Journal of Structural Geology*, *69*(A), 163–178. https://doi.org/10.1016/j.jsg.2014.10.007

Best, M. G., Christiansen, E. H., Deino, A. L., Gromme, S., Hart, G. L., & Tingey, D. G. (2013). The 36–18 Ma Indian Peak–Caliente ignimbrite field and calderas, southeastern Great Basin, USA: Multicyclic super-eruptions. *Geosphere*, *9*(4), 864–950. https://doi.org/10.1130/GES00902.1

Biek, R. F., Hacker, D. B., & Rowley, P. D. (2015). New constraints on the extent, age, and emplacement history of the early Miocene Markagunt Megabreccia, southwest Utah–One of the world's largest subaerial gravity slides. In J. S. MacLean, R. F. Biek, & J. E. Hunton (Eds.), *Geology of Utah's Far South* (Vol. 43, pp. 565–598). Utah Geological Association Publication.

Biek, R. F., Rowley, P. D., & Hacker, D. B. (2019). The Gigantic Markagunt and Sevier gravity slides resulting from mid-cenozoic catastrophic mega-scale failure of the Marysvale volcanic field. *Geological Society of America Field Trip Guide*, *56*, 1–108. https://doi.org/10.1130/2019.0056(01)

Billi, A., Salvini, F., & Storti, F. (2003). The damage zone-fault core transition in carbonate rocks: Implications for fault growth, structure, and permeability. *Journal of Structural Geology*, *25*(11), 1779–1794. https://doi.org/10.1016/S0191-8141(03)00037-3

Billi, A., & Storti, F. (2004). Fractal distribution of particle size in carbonate cataclastic rocks from the core of a regional strike-slip fault zone. *Tectonophysics*, *384*(1–4), 115–128. https://doi.org/10.1017/j.tecto.2004.03.015

Blenkinsop, T. G. (1991). Cataclasis and processes of particle size reduction. *Pure and Applied Geophysics*, *136*(1), 59–86. https://doi.org/10.1007/BF00878888

Boyer, S. E., & Hossack, J. R. (1992). Structural features and emplacement of surficial gravity-slide sheets, northern Idaho-Wyoming thrust belt. In P. K. Link, M. A. Kuntz, & L. B. Platt (Eds.), *Regional geology of eastern Idaho and western Wyoming* (Vol. 179). Geological Society of America Memoir. https://doi.org/10.1130/MEM179-p197

Braunagel, M. (2023). Sevier Gravity Slide 3D Outcrop Models (Version 1). [Dataset]. figshare. https://doi.org/10.6084/m9.figshare.22594063.v1

Braunagel, M. J., Griffith, W. A., Biek, R., Hacker, D., Malone, D., & Rivera, T. (2021). *Emplacement of the Marysvale gravity slide complex aided by thermal pressurization of shear zone fluids*. AGU Fall Meeting abstracts. NH43A-08.

Byerlee, J. (1978). Friction of rocks. In J. D. Byerlee & M. Wyss (Eds.), *Rock friction and earthquake prediction, Contributions to current research in Geophysics* (Vol. 6). https://doi.org/10.1007/978-3-0348-7182-2_4

Campbell, C. S., Cleary, P. W., & Hopkins, M. (1995). Large-scale landslide simulations: Global deformation velocities and basal friction. *Journal of Geophysical Research*, *100*(B5), 8267–8283. https://doi.org/10.1029/94JB00937

Cardozo, N., & Allmendinger, R. W. (2013). Spherical projections with OSX Stereonet. *Computers & Geosciences*, *51*(0), 193–205. https://doi.org/10.1016/j.cageo.2012.07.021

Chester, J. S., Chester, F. M., & Kronenberg, A. K. (2005). Fracture surface energy of the Punchbowl fault, San Andreas system, California. *Nature*, *437*(7055), 133–136. https://doi.org/10.1038/nature03942

Collins, G. S., & Melosh, H. J. (2003). Acoustic fluidization and the extraordinary mobility of sturzstroms. *Journal of Geophysical Research*, *108*(B10). https://doi.org/10.1029/2003JB002465

Craddock, J. P., Geary, J., & Malone, D. H. (2012). Vertical Injectites of detachment carbonate Ultracataclasite at White Mountain, Heart Mountain Detachment, Wyoming. *Geology*, *40*(5), 463–466. https://doi.org/10.1130/G32734.1

Craddock, J. P., Malone, D. H., Magloughlin, J., Cook, A. L., Rieser, M. E., & Doyle, J. R. (2009). Dynamics of the emplacement of the Heart Mountain allochthon at White Mountain: Constraints from calcite twinning strains, anisotropy of magnetic susceptibility, and thermodynamic calculations. *GSA Bulletin*, *121*(5–6), 919–938. https://doi.org/10.1130/B26340

Davies, T. R., & McSaveney, M. J. (2009). The role of rock fragmentation in the motion of large landslides. *Engineering Geology*, *109*(1–2), 67–79. https://doi.org/10.1016/j.enggeo.2008.11.004

Di Toro, G., Han, R., Hirose, T., De Paola, N., Nielsen, S., Mizoguchi, K., et al. (2011). Fault lubrication during earthquakes. *Nature*, *471*(7339), 494–498. https://doi.org/10.1038/nature09838

Dufresne, A., Siebert, L., & Bernard, B. (2021). Distribution and geometric parameters of volcanic debris Avalanche deposits. In M. Roverto, A. Dufresne, & J. Proctor (Eds.), *Volcanic debris Avalanches, Advances in volcanology*. https://doi.org/10.1007/978-3-030-57411-6_4

Ferri, F., Di Toro, G., Hirose, T., Han, R., Noda, H., Shimamoto, T., et al. (2011). Low-to high-velocity frictional properties of the clay-rich gouges from the slipping zone of the 1963 Vaiont slide, northern Italy. *Journal of Geophysical Research*, *116*(B9), B09208. https://doi.org/10.1029/2011JB008338

Fleck, R. J., Anderson, J. J., & Rowley, P. D. (1975). Chronology of mid-Tertiary volcanism in the High Plateaus region of Utah. In J. J. Anderson, P. D. Rowley, R. J. Fleck, & A. E. M. Nairn (Eds.), *Cenozoic geology of southwestern High Plateaus of Utah* (Vol. 160, pp. 53–62). Geological Society of America Special Paper. https://doi.org/10.1130/SPE160

Frost, E., Dolan, J., Sammis, C., Hacker, B., Cole, J., & Ratschbacher, L. (2009). Progressive strain localization in a major strike-slip fault exhumed from midseismogenic depths: Structural observations from the Salzach-Ennstal-Mariazell-Puchberg fault system, Austria. *Journal of Geophysical Research*, *114*(B04406), B04406. https://doi.org/10.1029/2008JB005763

Goren, L., & Aharonov, E. (2007). Long runout landslides: The role of frictional heating and hydraulic diffusivity. *Geophysical Research Letters*, *34*(7), L07301. https://doi.org/10.1029/2006GL028895

Goren, L., & Aharonov, E. (2009). On the stability of landslides: A thermo-poro- elastic approach. *Earth and Planetary Science Letters*, *277*(3–4), 365–372. https://doi.org/10.1016/j.epsl.2008.11.002

Goren, L., Aharonov, E., & Anders, M. H. (2010). The long runout of the Heart Mountain landslide: Heating, pressurization, and carbonate decomposition. *Journal of Geophysical Research*, *115*(B10), B10210. https://doi.org/10.1029/2009JB007113

Hacker, D. B., Biek, R. F., & Rowley, P. D. (2014). Catastrophic emplacement of the gigantic Markagunt gravity slide, southwest Utah (USA): Implications for hazards associated with sector collapse of volcanic fields. *Geology*, *42*(11), 943–946. https://doi.org/10.1130/G35896.1

Hacker, D. B., Holm, D. K., Rowley, P. D., & Blank, H. R. (2002). Associated Miocene laccoliths, gravity slides, and volcanic rocks, Pine Valley Mountains and Iron Axis region, southwestern Utah. In W. R. Lund (Ed.), *Field guide to geologic excursions in southwestern Utah and adjacent areas of Arizona and Nevada: U.S* (Vol. 02–172, pp. 236–283). Geological Survey Open-File Report.

Hoiland, C., Hourigan, J., & Miller, E. (2022). Evidence for large departures from lithostatic pressure during Late Cretaceous metamorphism in the northern Snake Range metamorphic core complex, Nevada. In J. P. Craddock, D. H. Malone, B. Z. Foreman, & A. Konstantinou (Eds.), *Tectonic evolution of the Sevier-Laramide Hinterland, Thrust Belt, and Foreland, and Postorogenic Slab Rollback (180-20 Ma)*. Geological Society of America Special. Paper 555. https://doi.org/10.1130/2021.2555(07

Holliday, M. E., Rivera, T., Jicha, B., Trayler, R. B., Biek, R. F., Braunagel, M. J., et al. (2022). *Emplacement age of the Markagunt gravity slide in southwestern Utah, USA*. Terra Nova.

Jiang, T., Shao, J. F., Xu, W. Y., & Zhou, C. B. (2010). Experimental investigation and micromechanical analysis of damage and permeability variation in brittle rocks. *International Journal of Rock Mechanics and Mining Sciences*, *47*(5), 703–713. https://doi.org/10.1017/j.ijrmms.2010.05.003

Johnson, B. (1978). Blackhawk landslide, California, U.S.A. *Developments in Geotechnical Engineering*, *14*(A), 481–504. https://doi.org/10.1016/B978-0-444-41507-3.50022-2

Johnson, B. C., Campbell, C. S., & Melosh, H. J. (2016). The reduction of friction in long runout landslides as an emergent phenomenon. *Journal of Geophysical Research: Solid Earth*, *121*(5), 881–889. https://doi.org/10.1002/2015JF003751

Jolly, R. J. H., & Lonergan, L. (2002). Mechanisms and controls on the formation of sand intrusions. *Journal of the Geological Society*, *159*(5), 605–617. https://doi.org/10.1144/0016-764902-025

Komorowski, J. C., Glicken, H. X., & Sheridan, M. F. (1991). Secondary electron imagery of microcracks and hackly fracture surfaces in sand-size clasts from the 1980 Mount St. Helens debris-avalanche deposit: Implications for particle-particle interactions. *Geology*, *19*(3), 261–264. https://doi.org/10.1130/0091-7613(1991)019<0261:SEIOMA>2.3.CO;2

Lachenbruch, A. H. (1980). Frictional heating, fluid pressure, and the resistance to fault motion. *Journal of Geophysical Research*, *85*(B11), 6097–6112. https://doi.org/10.1029/JB085iB11p06097

Legros, F. (2002). The mobility of long-runout landslides. *Engineering Geology*, *63*(3–4), 301–331. https://doi.org/10.1016/S0013-7952(01)00090-4

Legros, F., Cantagrel, J.-M., & Devouard, B. D. (2000). Pseudotachylyte (Frictionite) at the Base of Arequipa Volcanic Landslide Deposit (Peru): Implications for emplacement mechanisms. *The Journal of Geology*, *108*(5), 601–611. https://doi.org/10.1086/314421

Magloughlin, J. F., & Spray, J. G. (1992). Frictional melting processes and products in geologic materials: Introduction and discussion. *Tectonophysics*, *204*(3–4), 197–206. https://doi.org/10.1016/0040-1951(92)90307-R

Malone, D. H. (1995). Very large debris-avalanche deposit within the Eocene volcanic succession of the northeastern Absaroka Range, Wyoming. *Geology*, *23*(7), 661–664. https://doi.org/10.1130/0091-7613(1995)023<661:VLDADW>2.3.CO;2

Malone, D. H., Craddock, J. P., Anders, M. H., & Wulff, A. P. (2014). Constraints on the emplacement age of the massive Heart Mountain Slide, Northwestern Wyoming. *The Journal of Geology*, *122*(6), 671–685. https://doi.org/10.1086/678279

Malone, D. H., Craddock, J. P., Schmitz, M. D., Kenderes, S., Kraushaar, B., Murphey, C. J., et al. (2017). Volcanic initiation of the Eocene Heart Mountain Slide, Wyoming, USA. *The Journal of Geology*, *125*(4), 439–457. https://doi.org/10.1086/692328

Marrett, R., & Allmendinger, R. W. (1990). Kinematic analysis of fault-slip data. *Journal of Structural Geology*, *12*(8), 973–986. https://doi.org/10.1016/0191-8141(90)90093-E

Masch, L., Wenk, H. R., & Preuss, E. (1985). Electron microscopy study of hyalomylonites – Evidence for frictional melting in landslides. *Tectonophysics*, *115*(1–2), 131–160. https://doi.org/10.1016/0040-1951(85)90103-9

Mase, C. W., & Smith, L. (1985). Effects of frictional heating on the thermal, hydrologic, and mechanical response of a fault. *Journal of Geophysical Research*, *92*(B7), 6249–6272. https://doi.org/10.1029/JB092iB07p06249

Mayback, D. F., Braunagel, M. J., Malone, D. H., Griffith, W. A., Holliday, M. E., Rivera, T. A., et al. (2022). The concept of tectonic provenance: Case study of the gigantic Markagunt gravity slide basal layer. *Terra Nova*, *34*(5), 449–457. https://doi.org/10.1111/ter.12608

Melosh, H. J. (1979). Acoustic fluidization: A new geologic process? *Journal of Geophysical Research*, *84*(B13), 7513–7520. https://doi.org/10.1029/JB084iB13p07513

Mitchell, T. M., Smith, S. A. F., Anders, M. H., Di Toro, G., Nielsen, S., Cavallo, A., & Beard, A. D. (2015). Catastrophic emplacement of giant landslides aided by thermal decomposition: Heart Mountain, Wyoming. *Earth and Planetary Science Letters*, *411*, 199–207. https://doi.org/10.1016/j.epsl.2014.10.051

Otsu, N. (1979). A threshold selection method from gray-level histograms. *IEEE Transactions on Systems, Man, and Cybernetics*, *9*(1), 62–66. https://doi.org/10.1109/TSMC.1979.4310076

Palmer, B. A., & Walton, A. W. (1990). Accumulation of volcaniclastic aprons in the Mount Dutton Formation (Oligocene-Miocene), Marysvale volcanic field, Utah. *GSA Bulletin*, *102*(6), 734–748. https://doi.org/10.1130/0016-7606(1990)102<0734:AOVAIT>2.3.CO;2

Pollet, N., & Schneider, J.-L. M. (2004). Dynamic disintegration processes accompanying transport of the Holocene Flims sturzstrom (Swiss Alps). *Earth and Planetary Science Letters*, *221*(1–4), 433–448. https://doi.org/10.1016/S0012-821X(04)00071-8

Pringle, J. K., Howell, J. A., Hodgetts, D., Westerman, A. R., & Hodgson, D. M. (2006). Virtual outcrop models of petroleum reservoir analogies: A review of the current state-of-the-art. *First Break*, *24*(3). https://doi.org/10.3997/1365-2397.2006005

Rice, J. R. (2006). Heating and weakening of faults during earthquake slip. *Journal of Geophysical Research*, *111*(B5). https://doi.org/10.1029/2005JB004006

Rowe, C. D., & Griffith, W. A. (2015). Do faults preserve a record of seismic slip? A second opinion. *Journal of Structural Geology*, *78*, 1–26. https://doi.org/10.1016/j.jsg.2015.06.006

Rowe, C. D., Kirkpatrick, J. D., & Brodsky, E. E. (2012). Fault rock injections record paleo-earthquakes. *Earth and Planetary Science Letters*, *335–336*, 154–166. https://doi.org/10.1016/j.epsl.2012.04.015

Rowley, P. D., Cunningham, C. G., Steven, T. A., Mehnert, H. H., & Naeser, C. W. (1998). Cenozoic igneous and tectonic setting of the Marysvale volcanic field, and its relation to other igneous centers in Utah and Nevada. In J. D. Friedmann & A. C. Huffman (Eds.), *Laccolith complexes of southeastern Utah–Time of emplacement and Tectonic settings–Workshop proceedings: U.S* (Vol. 2158, pp. 167–202). Geological Survey Bulletin.

Rowley, P. D., Cunningham, C. G., Steven, T. A., Workman, J. B., Anderson, J. J., & Theissen, K. M. (2002). Geologic map of the Central Marysvale volcanic field, southwestern Utah. In *U.S. Geological Survey Geologic Investigation Series Map I-2645-A*.

Rowley, P. D., Mehnert, H. H., Naeser, C. W., Snee, L. W., Cunningham, C. G., Steven, T. A., et al. (1994). *Isotopic ages and stratigraphy of Cenozoic rocks of the Marysvale volcanic field and adjacent areas, West-Central Utah* (Vol. 2071, pp. 1–35). U.S. Geological Survey Bulletin. https://doi.org/10.3133/b2071

Sable, E. G., & Maldonado, F. (1997). The Brian Head Formation (revised) and selected Tertiary sedimentary rock units, Markagunt Plateau and adjacent areas, southwestern Utah. In F. Maldonado & L. D. Nealey (Eds.), *Geologic studies in the Basin and Range-Colorado Plateau transition zone in Southeastern Nevada, Southwestern Utah, and Northwestern Arizona: U.S* (Vol. 2153, pp. 7–26). Geological Survey Bulletin.

Sammis, C. G., & King, G. C. P. (2007). Mechanical origin of power law scaling in fault zone rock. *Geophysical Research Letters*, *34*(4), L04312. https://doi.org/10.1029/2006GL028548

Sammis, C. G., King, G. C. P., & Biegel, R. (1987). The kinematics of gouge deformation. *Pure and Applied Geophysics*, *125*(5), 777–812. https://doi.org/10.1007/BF00878033

Schneider, J.-L., & Fisher, R. V. (1998). Transport and emplacement mechanisms of large volcanic debris avalanches: Evidence from the northwest sector of Cantal Volcano (France). *Journal of Volcanology and Geothermal Research*, *83*(1–2), 141–165. https://doi.org/10.1016/S0377-0273(98)00016-X

Shaller, P. J., Doroudian, M., & Hart, M. W. (2020). The Eureka Valley landslide: Evidence of a dual failure mechanism for a long-runout landslide. https://doi.org/10.2113/2020/8860819

Shaller, P. J., & Smith-Shaller, A. (1996). Review of proposed mechanisms for Sturztroms (long-runout landslides). In *Sturzstroms and detachment faults, Anza-Borrego Desert State Park, California* (pp. 185–202). South Coast Geological Society.

Shreve, R. L. (1968). *The Blackhawk landslide* (Vol. 108). The Geological Society of America Special Paper. https://doi.org/10.1130/SPE108-p1

Siebert, L. (2002). Landslides resulting from structural failures of volcanoes. In S. G. Evans & J. V. DeGraff (Eds.), *Catastrophic landslides: Effects, occurrences, and mechanisms: GSA reviews in engineering geology* (Vol. 15, pp. 209–235). https://doi.org/10.1130/REG15-p209

Smith, Z. D., & Maxwell, D. J. (2021). Constructing vertical measurement logs using UAV-based photogrammetry: Applications for multi-scale high-resolution analysis of coarse-grained volcaniclastic stratigraphy. *Journal of Volcanology and Geothermal Research*, *409*, 107122. https://doi.org/10.1016/j.jvolgeores.2020.107122

Spray, J. G. (1995). Pseudotachylyte controversy: Fact or friction? *Geology*, *23*(12), 1119–1122. https://doi.org/10.1130/0091-7613(1995)023<1119:PCFOF>2.3.CO;2

Steven, T. A., Rowley, P. D., & Cunningham, C. G. (1984). Calderas of the Marysvale volcanic field, West-Central Utah. *Journal of Geophysical Research*, *89*(B10), 8751–8764. https://doi.org/10.1029/JB089iB10p08751

Thiele, S. T., Grose, L., Samsu, A., Micklethwaite, S., Vollgger, S. A., & Cruden, A. R. (2017). Rapid, semi-automatic fracture and contact mapping for point clouds, images, and geophysical data. *Solid Earth*, *8*(6), 1241–1253. https://doi.org/10.5194/se-8-1241-2017

Thompson, L. M., & Spray, J. G. (1996). Pseudotachylyte petrogenesis: Constraints from the Sudbury impact structure. *Contributions to Mineralogy and Petrology*, *125*(4), 359–374. https://doi.org/10.1007/s004100050228

Vardoulakis, I. (2002). Dynamic thermos-poro-mechanical analysis of catastrophic landslides. *Géotechnique*, *52*(3), 157–171. https://doi.org/10.1680/geot.2002.52.3.157

Viesca, R. C., & Garagash, D. I. (2015). Ubiquitous weakening of faults due to thermal pressurization. *Nature Geoscience*, *8*(11), 875–879. https://doi.org/10.1038/ngeo2554

Weidinger, J. T., Korup, O., Munack, H., Altenberger, U., Dunning, S. A., Tippelt, G., & Lottermoser, W. (2014). Giant rockslides from the inside. *Earth and Planetary Science Letters*, *389*, 62–73. https://doi.org/10.1016/j.epsl.2013.12.017

Yarnold, J. C., & Lombard, J. P. (1989). A facies model for large rock-avalanches deposits formed in dry climates. In I. P. Colburn, P. L. Abbott, & J. Minch (Eds.), *Conglomerates in basin analysis: A symposium dedicated to A.O. Woodford* (Vol. 62, pp. 9–31). Pacific Section S.E.P.M.

Zamanialavijeh, N., Hosseinzadehsabeti, E., Ferré, E. C., Hacker, D. B., Biedermann, A. R., & Biek, R. F. (2021). Kinematics of frictional melts at the base of the world's largest terrestrial landslide: Markagunt gravity slide, southwest Utah, United States. *Journal of Structural Geology*, *153*, 104448. https://doi.org/10.1017/j.jsg.2021.104448